Characterization of *eomesa*+ retinal ganglion cells in zebrafish

A Thesis

submitted to

Indian Institute of Science Education and Research Pune in partial fulfilment of the requirements for the BS-MS Dual Degree Programme

by

UYYASHRINILA P

Indian Institute of Science Education and Research Pune

Dr. Homi Bhabha Road, Pashan, Pune 411008, INDIA.

Under the guidance of

Supervisor: Prof. Dr. Herwig Baier

Max Planck Institute for Biological Intelligence, Martinsried, Germany

From May 2024 to Mar 2025

INDIAN INSTITUTE OF SCIENCE EDUCATION AND RESEARCH PUNE

Certificate

This is to certify that this dissertation entitled 'Characterization of *eomesa*+ retinal ganglion cells in zebrafish' towards the partial fulfilment of the BS-MS dual degree programme at the Indian Institute of Science Education and Research, Pune represents study/work carried out by Uyyashrinila P at Max Planck Institute for Biological Intelligence under the supervision of Prof. Dr. Herwig Baier, Director, Department of Genes-Circuits-Behavior during the academic year 2024-2025.

Prof. Dr. Herwig Baier

Thesis Advisory Committee:

Prof. Dr. Herwig Baier

Max Planck Institute for Biological Intelligence

Prof. Dr. Girish Ratnaparkhi

Indian Institute of Science Education and Research, Pune

This thesis is dedicated to my father, Dr. S.S. Pandiarajan

For his undying mentorship and love

For his unlimited sacrifices to get me here and now

For the scientific temper he instilled

For dealing with my absence, patient despite unthrilled

For motivating me to pursue my career

Without whom I wouldn't persevere

Declaration

I hereby declare that the matter embodied in the report entitled "Characterization of *eomesa*+ retinal ganglion cells in zebrafish" are the results of the work carried out by me at the Indian Institute of Science Education & Research (IISER) Pune, under the supervision of Prof. Dr. Herwig Baier, Max Planck Institute for Biological Intelligence, and the same has not been submitted elsewhere for any other degree. Wherever others contribute, every effort is made to indicate this clearly, with due reference to the literature and acknowledgement of collaborative research and discussions.

UYYASHRINILA P

20201124

Table of contents

List of Tables

List of Figures

Abstract

Retinal ganglion cells (RGCs) play a bottleneck role in visual processing, as they are the only output neurons of the eye that allow the flow of all the visual information to the visual centers in the brain. In Kölsch et al. (2021), using zebrafish as the model organism, it was determined by computational analysis of transcriptional profiles that there are around 30 different RGC types in zebrafish. Strikingly, the set of RGCs in larvae differs strongly from that in adults. To see how RGCs develop into different suptypes and how the set of subtypes changes over time, this project focused on the differentiation of one early transcriptomic subcluster, LC13, from Kölsch et al. LC13 expresses both the transcription factors *eomesa* and *onecut1*, but differentiates into larval and adult clusters that express either one or both of the transcription factors.

To determine a suitable developmental model for LC13, this project aimed to match transcriptomic RGC types to their morphology in a temporal fashion. To achieve this, the morphology of *eomesa*+ RGCs in the larval and juvenile stages were catalogued by sparse labelling and imaging. This study identified 12 different morphotypes of *eomesa*+ RGCs in six dpf old zebrafish with seven different types based on dendritic morphology only. In comparison, only five different dendritic morphotypes of *eomesa*+ RGCs were found in juvenile stages suggesting that two types are removed over the course of development.

Additionally, the project aimed to understand the role of LC13 related RGCs in visually guided responses, with phototaxis as an example. Zebrafish adults are photophobic while larvae show positive phototaxis. Further, selective ablation of *eomesa*+ RGCs in zebrafish larvae led to impaired phototaxis (Kölsch et al. (2021)). Combining these two observations, we hypothesized that the change in the transcriptomic and morphological types of LC13 related RGCs are relevant for the phototactic switch in zebrafish. Chemogenetic ablation of different LC13 related RGCs, followed by phototaxis assay revealed that both *onecut1*+ and *eomesa*+ RGCs are relevant for phototactic responses in seven dpf old zebrafish.

Acknowledgements

This dissertation project has been a thrilling scientific pursuit that shaped me personally and professionally. This would not have been possible if not for the contribution of people who deserve my heartfelt thanks:

Firstly, I would like to thank Prof. Dr. Herwig Baier for giving me the opportunity to work on this project and for his invaluable guidance throughout crucial to the development and continuation of this project. I would also like to express my gratitude to Prof. Dr. Girish Ratnaparkhi, my expert, for his inputs and support. I am thankful to IISER Pune and MPI-BI for this collaborative program that enabled my thesis. I would also like to appreciate the financial assistance offered by INSPIRE-SHE and Infosys scholarships during my academic education in IISER Pune.

I would like to express my heartfelt gratitude to Dr. Eva Laurell for her patient training and excellent mentorship that made this project possible. Her constant support, scientific and personal, has kept me going. All the lessons I learnt from her will stick with me for life. I would like to acknowledge her, Martin and Irene for their direct contributions to this project. I am thankful to Anne for all the administrative support. I am grateful to the Max Planck Institute for Biological Intelligence (MPI-BI) for all the facilities provided, especially the Fish Facility, Imaging Facility, Guesthouse Facility and the IT team. I would like to thank all my lab members for creating a pleasant and intellectually stimulating lab environment. Special thanks to Joyce and Swantje for always making me feel included.

I would like to thank my parents- Meenal and Pandiarajan, Uma Sushil Kumar and all my family members for equipping me with all the resources and emotional support required to navigate life abroad. I would like to express my gratitude to Nisarg for his constant practical and moral support in overcoming all the challenges I faced in Munich.

I would like to thank all my wonderful friends in MPI for making me feel at home, especially my roommate, Vaishnavi, for always including me in her adventurous plans. Last but not the least, I would like to thank all my friends from home- Sandhiya, Somdatta, Santhosh, Atharva and Sumanth for supporting me through it all despite the distance.

Contributions

Contributor name	Contributor role
HB, EL, UP	Conceptualization Ideas
UP, EL	Methodology
MP, UP	Software
UP	Validation
UP	Formal analysis
UP, EL	Investigation
EL, IA, MP	Resources
UP	Data Curation
UP	Writing - original draft preparation
EL, HB	Writing - review and editing
UP, EL, MA	Visualization
EL, HB	Supervision
HB	Project administration
HB	Funding acquisition

Contributor name

EL- Eva Laurell

HB- Herwig Baier

IA- Irene Arnold-Ammer

MA- Mariam Al Kassar

MP- Martin Privat

UP- Uyyashrinila P

Chapter 1: Introduction

1.1. Why study the visual system in zebrafish?

Studying neural circuits is intriguing because the intrinsic properties of neurons and their complex connections give rise to the wide repertoire of behavior seen in different animals. Understanding this emergent property will require deciphering how the transcriptomic, morphological and anatomical aspects of neural circuits correlate with their ethological relevance. This is one of the major questions in systems neuroscience. The visual system, a well studied sensory system that perceives and processes visual stimuli from our surroundings leading to visually guided behavior, is an interesting model to pursue this question. The retina, the preprocessor of visual information, is easily accessible due to its anatomical separation from the brain and it is relatively simple to study as it has only six different types of neurons highly organized in laminar layers.[3][4]

Zebrafish (*Danio rerio*) is chosen as a model organism for studying the visual system, because despite diverging from mammals many million years ago, they share the conserved vertebrate retinal architecture and development.[7] The development of their visual system is rapid and a wide range of behaviors is observed starting from five days post fertilization (dpf).[8] Apart from this, they confer experimental advantages by being easy to breed and maintain at low costs. Genetic modifications are also easy to implement in zebrafish allowing experimental manipulations. Easy availability of transgenic lines helps acquire targeted access of particular cell types and the transparent larvae can be imaged in vivo for structure and function. [9]

1.2. The zebrafish retina

The innermost layer of the eye called retina is where visual stimuli are converted into neuronal signals for perception[10]. It is made up of an evolutionarily conserved[7] intricate neural network layered by cells of six types: photoreceptors, bipolar cells, retinal ganglion cells, horizontal cells, amacrine cells and Müller glia cells. The cells are organized in three nuclear layers containing cell bodies and two plexiform layers containing synaptic connections. These layers are stacked in the order: outer nuclear

layer (ONL), outer plexiform layer (OPL), inner nuclear layer (INL), inner plexiform layer (IPL) and ganglion cell layer (GCL) from nasal to temporal (Fig. 1A). [10][11]

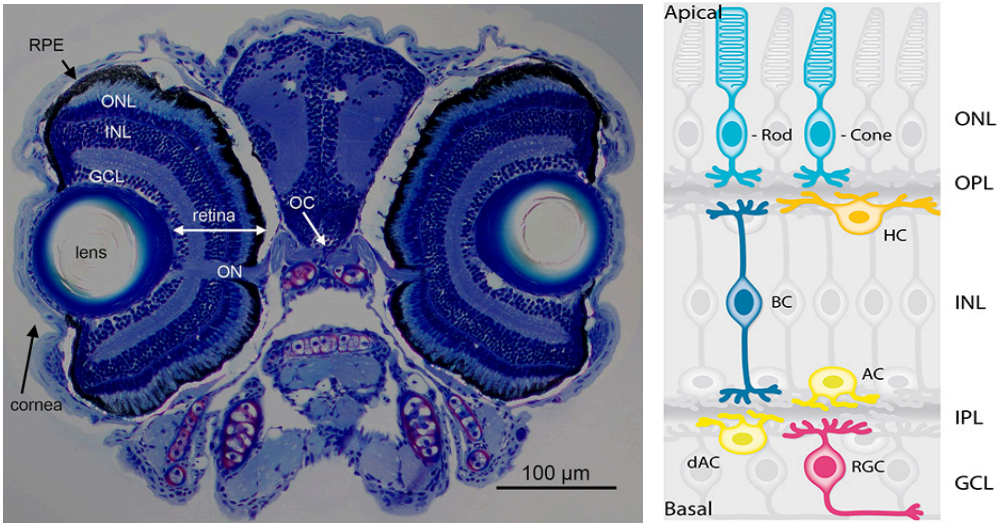

A B

Fig. 1: (A) Organization of the retinal layers shown in a tissue section through the head of a six-day-old zebrafish larva. OC, optic chiasm; ON, optic nerve; ONL, outer nuclear layer; INL, inner nuclear layer; GCL, ganglion cell layer; RPE, retinal pigment epithelium. Fish Physiology 29, Academic Press (2010)[12]. (B) Mature retina in zebrafish showing organization of cell bodies and their neurites. Amacrine cells; AC; Horizontal cells; HC, Bipolar cells; BC, displaced amacrine cells; dAC, Retinal ganglion cells; RGC. Rana, Mauricio and Caren, 2018[13].

The photoreceptors have their soma in the ONL and form connections with horizontal cells (HCs) and bipolar cells (BCs) in the OPL. The INL is made up of soma of the interneurons: bipolar cells (BCs), HCs and amacrine cells (ACs). The BCs form connections with ACs and retinal ganglion cells (RGCs) in the IPL. The cell bodies of RGCs and some displaced ACs lie in the GCL. (Fig. 1B). The retina is an interesting neuronal structure to study because it extracts fine visual features from visual input via complex computation. Photoreceptors and RGCs act as sole input and output neurons for visual information, respectively, while BCs, ACs and HCs are different kinds of interneurons that help in modulating and processing the information received [10]. They achieve this via the intrinsic diversity of each cell type and the complex organization of the networks between them.

Rods and cones are the two types of photoreceptors. The rods are involved in vision at low light conditions while cones play a role in bright light vision[7]. There is one kind of rod and four kinds of cones in zebrafish retina[14]: UV sensing short single cones, blue-sensitive long single cones, green-sensitive accessory members and red-sensitive

principle members of double cones. Double cones are two electrically coupled cone cells joined together. The photoreceptors sense light and convert them into neural impulses through a visual transduction cascade.

BCs are glutamatergic interneurons with dendrites in ONL to receive inputs from photoreceptors and with axons in the INL to deliver this information to RGCs and ACs.[15] The rod BCs associate themselves with rod photoreceptors while the cone BCs associate themselves with cones. The two kinds of cone BCs are ON BCs that sense light enhancement and OFF BCs that sense light reduction.[16][17] Their functional diversity reflects in their morphological properties as well. The IPL is divided into five sublaminar structures- S1 to S5. The axons of ON BCs extend to the proximal region of IPL (S3-S5) while those of OFF BCs innervate the distal regions of the IPL (S1 and S2). Previous studies have shown that there are about 17 different morphological types of BCs in zebrafish adults[18][19]. In addition to photoreceptors and BCs, the OPL contains HCs, which form synaptic triads with both photoreceptors and bipolar cells which are inhibitory in nature.[20] HCs play an important role in refining the visual information like contrast enhancement[22] and color opponency[21].

The IPL contains synaptic connections between BCs, ACs and RGCs in several layers and is the major site of visual processing. ACs are GABAergic and glycinergic inhibitory interneurons found in the INL and GCL with the GCL ACs being exclusively GABAergic. There are about 28 kinds of ACs based on morphological diversity in zebrafish at just 120 hours post fertilization. [18][24] Each AC forms connections with a specific set of BCs and RGCs at specific sublaminar positions.They shape the receptive field structures of BCs and RGCs, modify their dynamic ranges and adaptive properties to functionally diversify the retinal output.[23]

The RGCs in the GCL receive inputs from BCs and ACs in the IPL and send axonal projections to different retinorecipient regions of the brain. RGC types are feature specific, because each RGC is an output channel for a specialized retinal circuit formed by distinct BCs and ACs that extract specific visual features[25] like orientation of an object[26], direction of motion[27] etc. In conclusion, the retina produces pre-processed information that can be used for the formation of images in higher brain centers or for visually guided non-image forming pathways.

The axons of RGCs exit the retina as the optic nerve that projects to the contralateral hemisphere via the optic chiasm. They project to ten distinct retinorecipient neuropils in the zebrafish brain called the arborization fields (AF) labelled from AF1 to AF10 from ventral to dorsal.[28][2]

AF10, also known as the optic tectum, contains four regions from superficial to deep called as the stratum opticum (SO), stratum fibrosum et griseum superficiale (SFGS), stratum griseum centrale (SGC) and stratum album centrale (SAC). There are two sublayers of SO and six sublayers of SFGS while SGC and SAC are single layers. Therefore, RGCs have eighteen potential innervation sites when tectal and extratectal layers are taken together.[29]

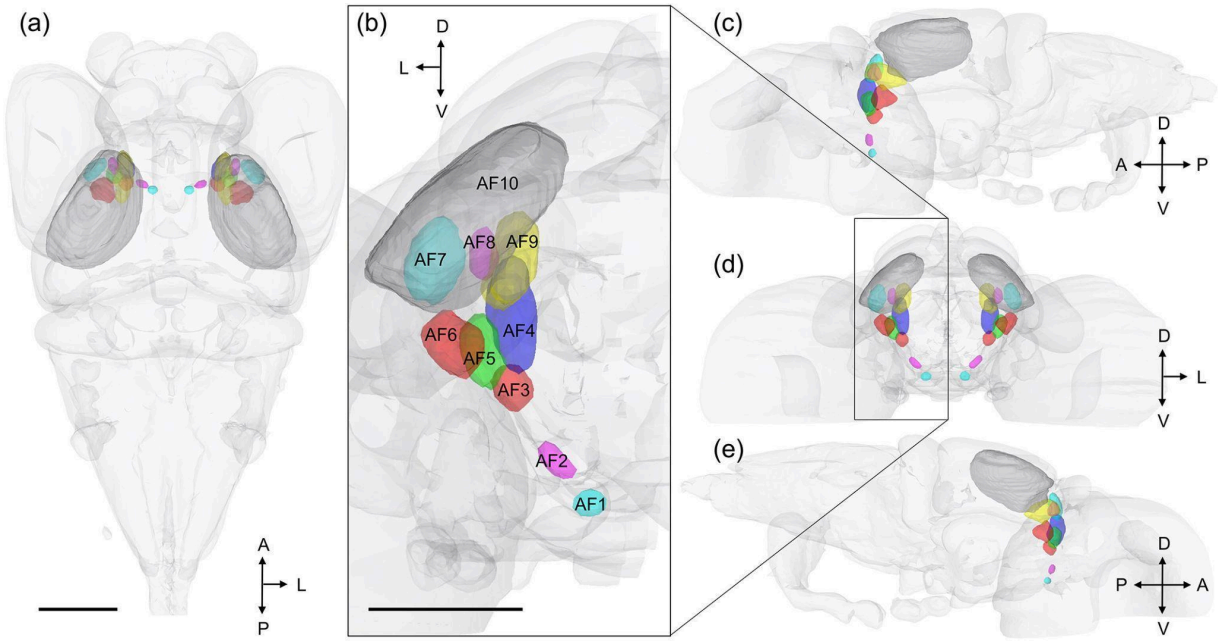

Fig. 2: 3D view of arborization fields (AFs) in the mapzebrain atlas by visualization tools at https://mapzebrain.org/home. Four different views of the AFs in the larval brain (light grey) are shown in (a), (c), (d) and (e). (b) Higher magnification of the AF-containing larval brain is shown. Scale bars in (a) and (b): 100 µm. A, anterior; P, posterior; D, dorsal; V, ventral; L, lateral. Baier and Wulliman, 2021[30].

There is a topographic organization to RGC projections, where the nasally positioned RGCs project to posterior parts of the tectum while temporally positioned RGCs project to anterior regions of the tectum[31]. AF6 mostly receives input from the dorsal retina while ventral retina projects to regions like the AF1, AF4 and AF8[2]. Interestingly, the

anatomical organization of RGC innervation also seems to correlate with function. For example, AF7 implied in prey hunting receives input mostly from temporal RGCs where prey detection is likely to occur[32].

1.3.The retinal projectome

Retinal ganglion cells (RGCs) play a bottleneck role in visual processing as they are the only output neurons of the eye that allow the flow of all the visual information to the higher brain centers. The retinal projectome, the comprehensive map of morphological connectivity patterns of the RGCs with the retinorecipient regions of the brain, is essential to understand how the visual system directs information to achieve correct behavioral responses. On analysing about 450 RGCs from seven dpf zebrafish larvae, Robles et al (2014)[2] has identified more than 50 distinct types of RGCs based on their dendritic and axonal morphology.

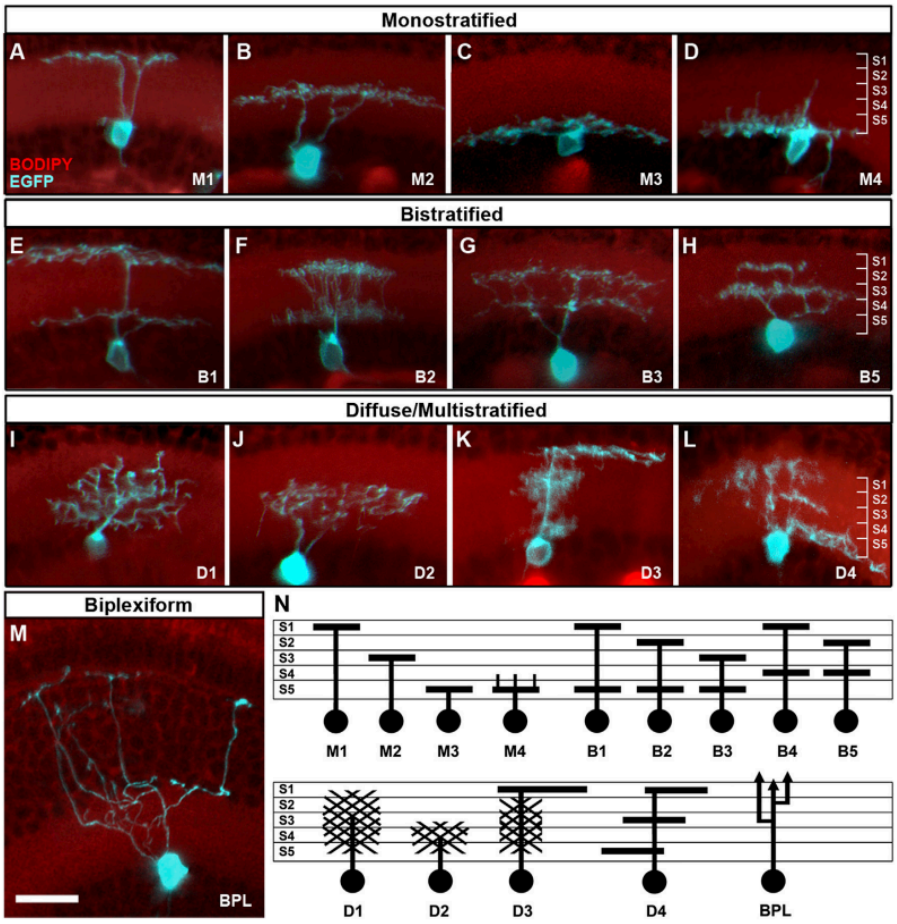

Fig. 3: RGC classification based on dendritic stratification patterns. Robles et al, 2014.

The five sublayers of the IPL are innervated by RGC dendrites to form synapses with BCs and ACs. This study identified 14 morphologically different dendritic classes of which there are four monostratified, five bistratified and four diffuse classes (Fig. 3). They are classified based on the depth of their laminar position (S1-S5) in the IPL. The four monostratified classes are Mono1-Mono4. Mono1 dendrites arborize in the S1 OFF layer while Mono2 dendrites arborize in the intermediate IPL. Mono3 and Mono4 have ON monostratified dendrites arborizing in S5 with the difference being the presence of a filopodia like structure extending into S3 and S4 in the case of Mono4. The five bistratified classes are Bi1-Bi5 which form stratifications in two distinct sublayers of the IPL. The four types of diffused dendritic classes are Diff1-Diff4. Diff1 dendrites are nonstratified occupying all layers of the IPL while Diff2 dendrites are limited to the ON layers, S3-S5. Diff3 dendrites arborize compactly in S2, S3 and S5 while also extending an asymmetric branch in S1. Diff4 dendrites have three arborizations specifically in S1, S3 and S5. A unique dendritic class is that of biplexiform RGCs, in which the dendrites extend till OPL passing through the IPL and the INL en route.[2]

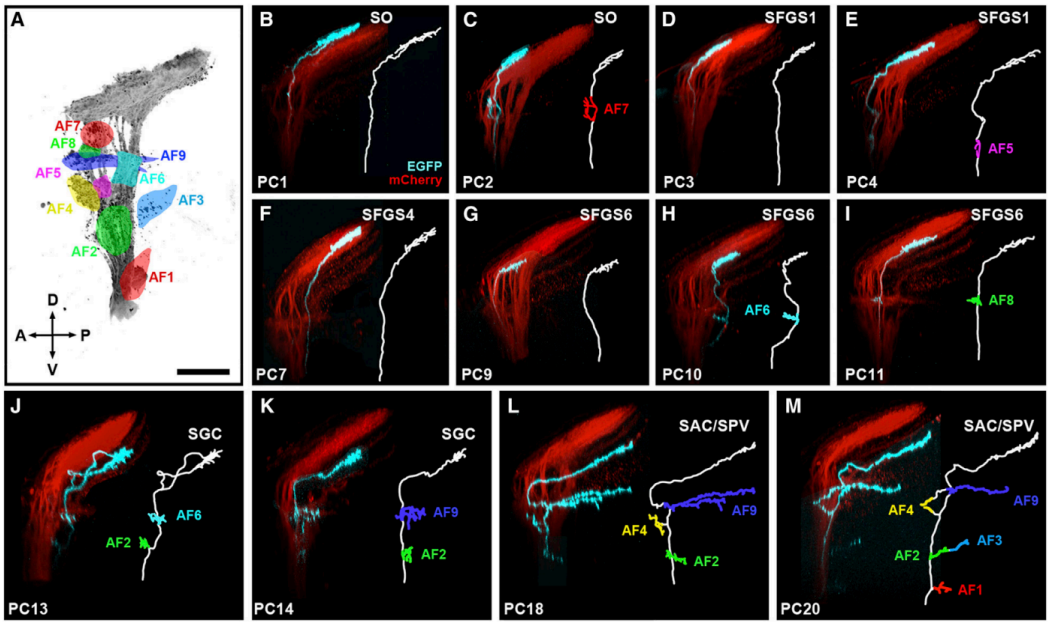

Fig. 4: Stereotyped RGC projection patterns. A, anterior; P, posterior; D, dorsal; V, ventral. Robles et al, 2014[2].

RGC axonal projections can be differentiated into 20 stereotyped projection classes (Fig. 4). 13 out of the 20 projection classes (PCs), representing 41% of the RGCs, innervate more than one AF, emphasizing the importance of signal divergence in

parallel processing. While a small fraction of axons terminate in AF9, the majority of axons comprising about 97% terminate in the tectum. All the other extratectal AFs are innervated en route to these two regions. Some projection classes exclusively innervate one sublayer of the tectum: PC1 innervates SO, PC3 innervates SFGS1 and PC5-PC8 innervate SFGS2-SFGS5 respectively. PC2 RGCs arborize in AF7 before terminating in SO while PC4 RGCs arborize AF5 and terminate in SFGS1. The SFGS6 layer of the tectum receives exclusive input from PC9 while it gets input integrated with that of AF6 and AF8 through PC10 and PC11, respectively. PCs that terminate in the SGC layer of the tectum also innervate one extratectal AF: AF2 by PC12; AF2 and AF6 by PC13 and AF2 and AF9 by PC14. The SAC is innervated by five PCs, with each arborizing at least two other AFs: AF1, AF2, AF3, AF4, and AF9 (PC20); AF1, AF2, AF4, and AF9 (PC19); AF2, AF4, and AF9 (PC18); AF2 and AF9 (PC16) and AF4 and AF9 (PC17). These constitute the PCs that terminate in the tectum. PC15 is a rare PC that forms axon collaterals in AF4 and terminates in AF9. The combination of dendritic stratification and axonal projection patterns define individual RGC morphologies. An axonal class can be correlated to upto eight dendritic classes while a dendritic class can be correlated with upto 12 axonal classes. Overall, the retinal projectome delivers a comprehensive RGCs classification based on their morphology. [2]

An interesting conclusion from this study[2] is that specific brain areas receive specific types of visual information since they are innervated by a distinct set of RGCs based on morphology. For example, a hypothesis would be that an AF implicated in converting prey sensing into capture behavior will be innervated specifically by prey sensing RGCs defined by a morphological identity. In this context, it is shown that the AF9 has two innervation zones- dorsal and ventral AF9. The dorsal AF9 receives axons from the ON RGCs while the ventral region receives axons from the OFF RGCs implicating functional relevance to this spatial segregation.[28] Another insight from this study is the use of parallel processing by the visual system from the prevalence of RGC PCs that innervate more than one brain area. For example, information on luminance in AF1 could be used for maintaining circadian rhythm while it can be used in the tectum to identify objects against changes in surrounding light levels. [2][30]

1.4.Transcriptional classification of RGCs

In Kölsch et al. (2021)[1], molecular catalogs of RGCs were assembled using single cell transcriptomics and bioinformatic clustering for both 5 dpf larvae and adult zebrafish. The transcriptional profiling involves the quantification of gene expression of RGCs at the transcription (mRNA) level using single cell RNA sequencing and clustering refers to grouping of RGCs together in accordance to their molecular similarities. Based on the expression of a specific set of transcription factors (TFs), 30 different RGC types of unique molecular identities were identified. The larval dataset showed a mixture of differentiated and immature RGCs with 23 larval clusters, about 67% of the RGCs at this stage, closely related to adult clusters. However, not all adult RGC types are present in larval stages suggesting that they might be responsible for behaviors that arise later in life like shoaling or photophobia. The most striking example of the difference between larval and adult transcriptomic RGCs is that of the clusters that express the TF, *Eomesa*. Five of the larval clusters express *eomesa* while it is present in only three adult clusters. The five larval clusters of *eomesa+ RGCs*, clusters 4, 18, 19, 25 and 26, exhibit unique molecular composition. Four of these clusters are closely related and express the neuropeptide *nmbb* while cluster 25 is unrelated to the rest. Interestingly, cluster 25 also does not have correspondence to any adult cluster. However, not much is known about the functional relevance of these subclusters and their development.

The difference between the transcriptomic sets of larval and adult RGCs, raises the question of the developmental model that RGC subtypes adopt. There are two different theoretical models that explain the development of RGC subtypes from larva to adult: the remodeling theory and the replacement theory (Fig. 4). If *onecut1+* RGC subtype A is found in larvae while subtype B is found in adults, the remodeling theory suggests that subtype A arises from an embryonic progenitor and gets transcriptomically and potentially morphologically and functionally remodeled to subtype B over time. On the contrary, the replacement theory suggests that adult progenitors give rise to the subtype B, which over time outnumbers the larval subtypes.

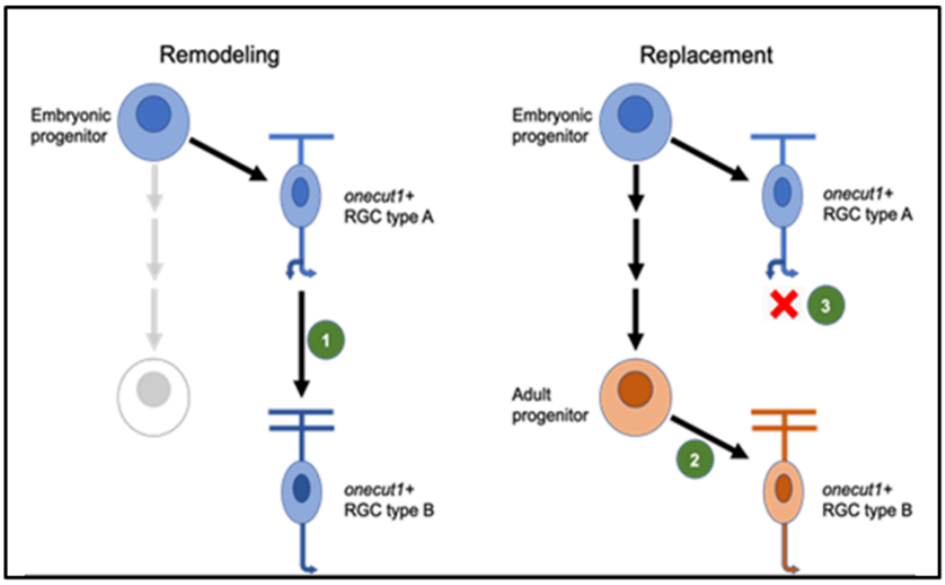

Fig. 5: Theoretical models of RGC subtype development, Herwig Baier and Karthik Shekar

Tracking the morphology of RGC subtypes over time will show how RGCs develop into different subtypes and how the set of subtypes changes over time given that there is a correlation between transcriptional and morphological subtypes of RGCs. There is substantial evidence that transcriptomic classes of RGCs also represent distinct RGC morphotypes from the analysis of *tbx20*+ RGCs. All RGCs that express the TF, *Tbx20* have mono stratification in the ON layer while their axon collaterals extend to AF4 and terminate in AF9 (Fig. 5).[1]

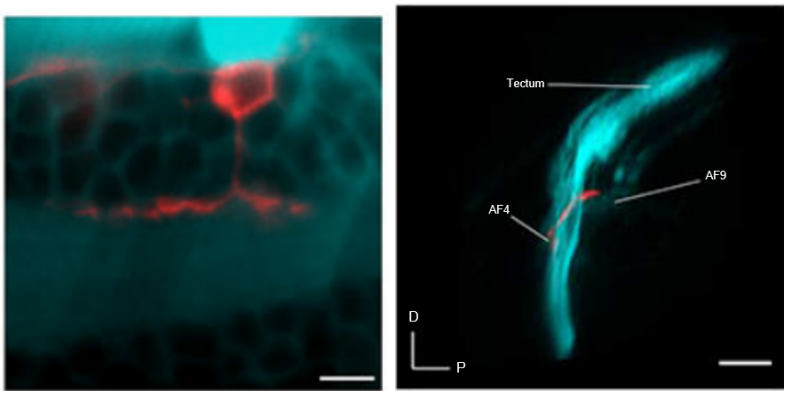

A B

Fig. 6: (A) Confocal images of the dendrites of *tbx20*+ RGC in a live *tbx20:Gal4, UAS:Dendra* larva. Scale bar, 5 µm. (B) Confocal image highlighting that *tbx20*+ RGC axons arborize in AF4 en route to AF9 in live *tbx20:Gal4, UAS:Dendra, isl2b:tagRFP* larva. D, dorsal; P, posterior. Scale bar, 50 µm. BODIPY (blue) and Dendra (red). Kölsch et al, 2021[1].

To decipher the suitable developmental model for RGCs, this project focuses on the *eomesa* subclass, the early larval cluster 13, by characterizing *eomesa*+ RGCs morphologically and functionally over time. RGCs of larval cluster 13 express the TFs, *eomesa* and/or *onecut1*. These differentiate into six transcriptomically different larval clusters: clusters 4, 8, 18, 19, 25 and 26. The molecular signature of these larval clusters (LC) and their corresponding adult clusters (AdC) is given in Table 1.

RGC precursors						
Early intermediate	LC13 **eomesa** **onecut1**					
Late intermediate	LC4 **eomesa** **onecut1** tbx20 opn4xa opn4b	LC8 **onecut1** opn4b (opn4xa)	LC18 **eomesa** opn4xa opn4b	LC19 **eomesa** **onecut1**	LC25 **eomesa**	LC26 **eomesa** **opn4b**
Mature	AdC24 **eomesa** **onecut1** tbx20 opn4xa opn4b	AdC26, AdC32 **onecut1** opn4b (opn4xa)	AdC30 **eomesa** opn4xa opn4b	AdC15 **eomesa** **onecut1**	X	X

Table 1: RGC differentiation. Yellow indicates both *eomesa* and *onecut1* expression, red indicates *onecut1* expression while green indicates *eomesa* expression. LC, larval cluster; AdC, adult cluster; X, absence of adult counterpart. Kölsch et al, 2021[1].

Some of the notable observations are the expression of *tbx20* along with *eomesa* and *onecut1* in LC4, the lack of corresponding adult cluster for LC25 and the expression of opsins in some of these LCs suggesting they could be ipRGCs.

1.5.*eomesa* expressing RGCs

In zebrafish, eomesodermin homolog a *(eomesa*), also known as Tbr2, is a T-box TF that is involved in several developmental processes like determination of dorsal identity, epiboly and gastrulation. It is expressed in various structures like the blastoderm, blastodisc, brain, eye and the immune system.[35] The ortholog of *eomesa*, *Eomes*, in mammals are expressed selectively, but not solely, in intrinsically photosensitive RGCs (ipRGCs).[36][37] ipRGCs were discovered when mice lacking photoreceptors could still retain visual functions like maintenance of circadian rhythms in response to light[39][40].

The expression of the photopigment, melanopsin, in this rare set of RGCs render them intrinsically light sensitive[41][34]. In mice, there are five types of RGCs with distinct dendritic stratifications: three monostratified in the ON layer (M2, M4 and M5), one monostratified in the OFF layer (M1) and one bistratified in the ON-OFF layers (M3).[42] The best studied subtype, M1 ipRGCs, are involved in circadian rhythm and pupillary light reflex.[43] ipRGCs are characterized by sustained and sluggish responses to light[44] and they mostly project to suprachiasmatic nucleus and olivary pretectal nucleus involved in circadian rhythm and pupillary light reflex respectively[43].

In zebrafish, there are five homologs of melanopsin (*opn4*): three are related to mammalian *opn4 (opn4.1*, *opn4a* and *opn4b*), while two are related to Xenopus *opn4x (opn4xa* and *opn4xb*).[45] From the transcriptional profiling done in Kölsch et al. (2021)[1], it is apparent that a subset of opsin expressing RGCs also expresses *eomesa*. Interestingly, the expression of opsins, *opn4xa* and *opn4b*, is limited to *eomesa*+ and *onecut1*+ RGCs types only. (Fig. 6). This molecular composition of ipRGCs is conserved in mice as well.[46][47]

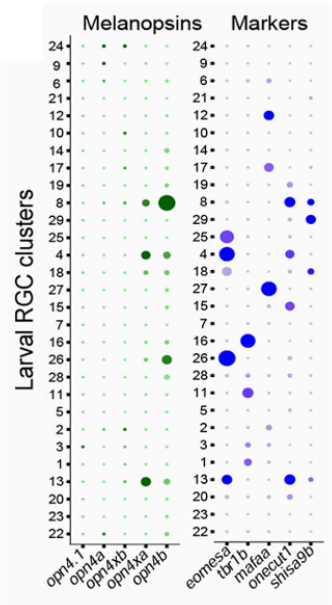

Fig. 7: Dotplots showing expression of melanopsin in larval transcriptomic RGC types. Left: *opn4xa* and *opn4b* are expressed in specific RGC clusters (rows) of the five melanopsin homologs (columns). Right: *opn4xa*+ and *opn4b*+ are expressed in *eomesa*+ RGC types. An *opn4xa*+ *opn4b*+ RGC type lacking *eomesa* shows the expression of *onecut1*. This data is preserved in adult RGC types. Kölsch et al., 2021[1].

Anatomically, the ventral retina contains an abundance of *eomesa*+ RGCs in both zebrafish and mice.[51][52] Additionally, *eomesa*+ RGCs also project to AF1, the only AF that forms connections with the hypothalamus, involved in non-image forming visual functions in zebrafish.[1][20] Selective ablation of *eomesa*+ RGCs using chemogenetic methods also led to phototaxis defect in zebrafish larvae[1]. All this evidence suggests that *eomesa*+ RGC subclass might contain ipRGCs in zebrafish as well. Very little is known about the morphological subtypes of *eomesa*+ RGCs and their functional relevance. The aim of this project is to morphologically characterize *eomesa*+ RGCs in zebrafish over different developmental stages and to correlate morphological properties to transcriptomically described subtypes as well as to conclude on their functional relevance. An intersectional approach is undertaken to label *eomesa*+ RGCs to study their morphology (Section 2.1, Chapter 2).

1.6. Role of *eomesa*+ RGCs in phototaxis

Phototaxis is a navigational behavior shown towards preferred light conditions. Zebrafish larvae show positive phototaxis from five dpf, while adults show negative phototaxis.[52][53][54] Very little is known about the molecular aspects behind this switch in phototaxis. The connection between the stark difference in transcriptomic RGC larval and adult clusters and such behavioral switches would be intriguing to study.

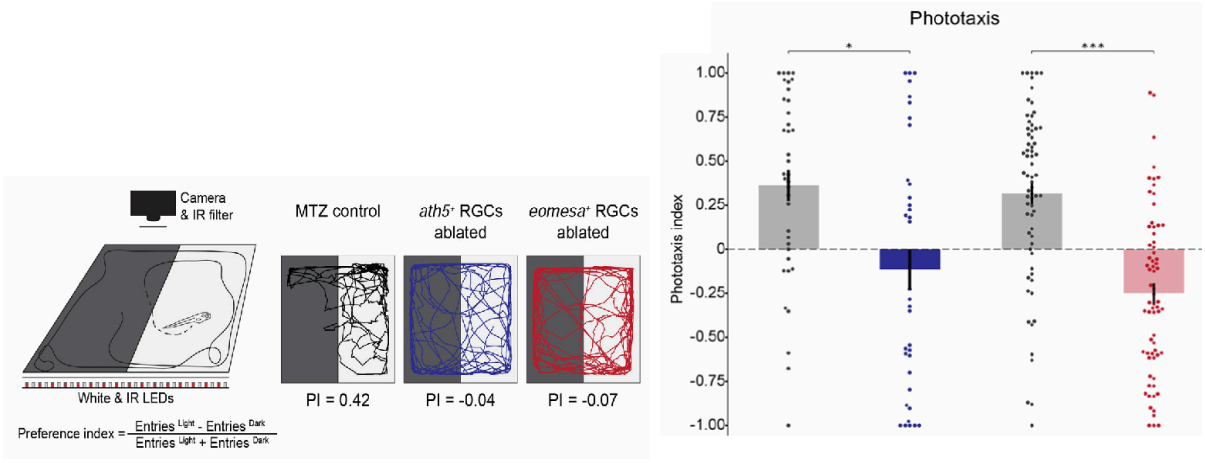

Fig. 11: (A) 7 dpf zebrafish larvae in the dark-light choice arena with their trajectories plotted for three groups: MTZ control (grey), *ath5*+ RGCs ablation (blue) and *eomesa*+ RGCs ablation (red). The equation for preference index (PI) is also shown. (B) The PI for the three groups is plotted: MTZ control (grey), *ath5*+ RGCs ablation (blue) and *eomesa*+ RGCs ablation (red).Kölsch et al., 2021[1].

Previously, Kölsch et al. (2021)[1] showed that selective ablation of *eomesa*+ RGCs using chemogenetic ablation methods conferred a phototactic defect in zebrafish larvae. Transgenic fish with genotype *ath5:Cre eomesa:QF2 QUAS:switch-tagRFP-epNTR* express nitroreductase (NTR) specifically in *eomesa*+ RGCs. NTR converts chemicals like metronidazole and ronidazole into cytotoxic compounds that selectively induce cell death in NTR expressing cells[55]. Following this chemogenetic ablation of *eomesa*+ RGCs selectively, a phototaxis assay is performed on these fish using a dark-light choice arena. The trajectory of larvae exposed to this half-illuminated arena is tracked and a preference index (PI) is plotted. This assay showed that *eomesa*+ RGCs are indeed needed for phototaxis since the fish with *eomesa*+ RGC ablation disrupted phototactic abilities as shown in Fig. 11.

1.7. Objectives

The two major research questions this project aims to pursue is: Do specific morphotypes of a particular transcriptomic RGC type correlate with specific functions? and How do RGC subtypes develop?

This project contributes to mapping the transcriptomic RGC cell types to their morphology over the course of different developmental stages with particular focus on the larval cluster, LC13 from Kölsch et al. (2021)[1]. Additionally, this project also aims to understand the functional relevance of these cell types in the context of phototaxis. This is achieved by the following objectives:

1. Sparse labeling and imaging of *eomesa*+ RGCs to catalogue their dendritic morphology and axonal projection patterns in larval and juvenile stages of zebrafish to understand RGC subtype development.
2. Assigning morphology to different LC13 RGC subtypes in zebrafish larvae by combining the sparse labelling approach with RNA *in-situ* hybridization chain reactions (HCRs)
3. Performing the phototaxis assay after chemogenetic ablation of *eomesa*+ RGC subtypes in zebrafish larvae, to understand their role in phototaxis.

Chapter 2: Materials and Methods

2.1. An intersectional approach is used to label *eomesa*+ RGCs

2.1.1. The Q system

To label *eomesa*+ RGCs, an intersectional approach combining the Q system and the Cre-loxP system is used.

The Q system is a binary system that serves as a genetic tool to express transgenes to modulate cell and circuit function efficiently. The Q system is based on the qa cluster of the fungus, *Neurospora crassa*, and contains four components: the transcriptional activator QF2, the enhancer QUAS, the repressor QS and a drug that counteracts the repressor, quinic acid. The 'driver' of this system, QF2 binds the 'reporter' QUAS to enable the expression of genes downstream to QUAS.[56] These two genes can be employed to express desired genes in cells of particular interest. For example, transgenic lines that express QF2 under a desired promoter of a gene of interest and a fluorescent protein downstream of QUAS, are used to visualize those particular transcriptional cell types. A transgenic line with QF2 under the *eomesa* promoter and tagRFP under QUAS (*eomesa:QF2 QUAS: tagRFP*) will label all the *eomesa*+ cells red.

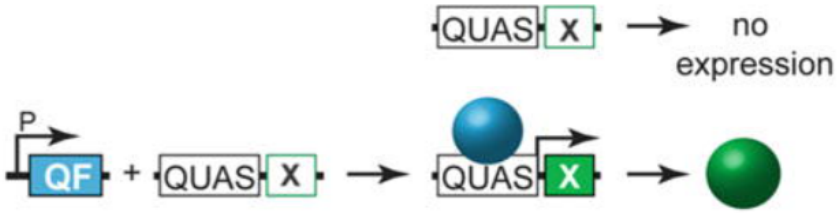

Fig. 8: Schematic of the Q binary expression system. Riabinina O, Potter CJ, 2016.[56]

2.1.2. The Cre-loxP system

The Cre-loxP system is a recombination system used for gene editing. Cre, named for causing recombination, is a recombinase enzyme isolated from P1 bacteriophage. loxP, named for locus of crossing over (x), are the binding sites of Cre. The DNA fragment in between two 34 bp loxP sites is called the 'floxed loci' which in the presence of Cre gets deleted due to the recombination it enabled between the loxP sites. If the Cre is

expressed in specific cells of interest using specific promoters, the deletion will take place in those specific cells.[57]

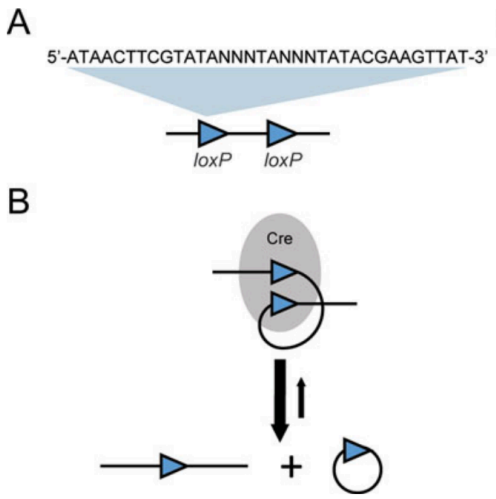

Fig. 9: The Cre-loxP genetic tool. (A) 34 bp loxP sequences (blue triangle) flanking gene of interest (B) Schematic showing the deletion of the desired gene in the presence of Cre recombinase (grey circle). McLellan MA, Rosenthal NA, Pinto AR. 2017. [57]

2.1.3. Intersectional labelling using the Q system and Cre-loxP system

Combining the Q system and the Cre-loxP system, specific subpopulation of cells can be targeted. For example, to limit the expression of a reporter protein to a specific subpopulation like RGCs, the Cre recombinase can be expressed under a pan-RGC marker like *ath5*. For this, two fluorescent reporter proteins are expressed under QUAS with one floxed in between the loxP sites and the other independent of the loxP sites.

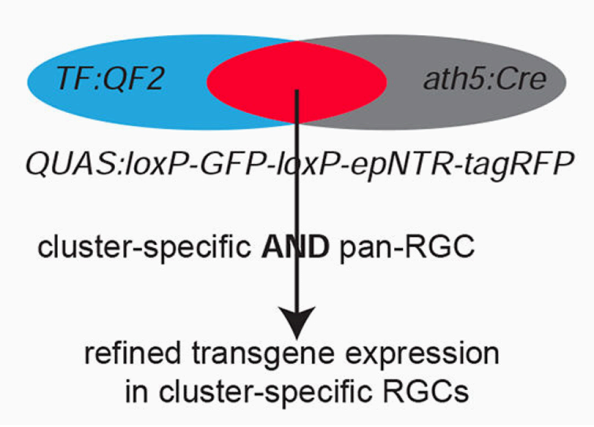

Fig. 10: Intersectional approach that enables targeted access to cluster specific RGCs. TF+ RGCs express GFP due to the *QUAS:switchNTR-RFP* construct. In the presence of pan-RGC, *ath5:Cre*, TF+ RGCs switch to RFP expression while other TF+ cells still express GFP. Kölsch et al., 2021[1].

For example, the transgenic line of genotype *ath5:Cre eomesa:QF2 QUAS: loxP_RFP_loxP_GFPcaax (*referred to as *QUAS:switchGFPcaax)* will label all *eomesa*+ cells red and only *eomesa*+ RGCs green. Note that the *ath5:Cre* construct can be coupled with the coldheart marker, *cmlc2:Cerulean*, that marks the heart with fluorescent cyan for identification. The progeny with the genotype *ath5:Cre-cmcl2:Cerulean eomesa:QF2 QUAS:tagRFP QUAS:switchGFPcaax* are selected based on the presence of Cre/coldheart marker, red *eomesa*+ cells and green *eomesa*+ expressing RGCs. This is the principle behind the intersectional approach to selectively label *eomesa*+ RGCs differently than the rest of *eomesa*+ cells.

2.2. Molecular cloning techniques

2.2.1. The Tol2 transposition system

To generate fish of genotype *ath5:Cre-cmcl2:Cerulean eomesa:QF2 QUAS:tagRFP QUAS:switchGFPcaax,* the *QUAS:switchGFPcaax* construct has to be introduced into zebrafish embryos resulting from the cross between transgenic fish expressing *eomesa:QF2 QUAS:tagRFP* and *ath5:Cre-cmlc2:Cerulean,* respectively. To achieve this, the Tol2 transposition system is used.

In zebrafish, the Tol2 transposition system consists of two elements: Tol2 transposon donor plasmid and transposase mRNA. The transposase enzyme expressed by the transposase mRNA leads to the transposition of the Tol2 transposon donor plasmid into the genome.[58] The desired construct, *QUAS:switchGFPcaax*, was cloned into the transposon donor plasmid to enable its genomic integration. The donor plasmid and the transposase mRNA are co-injected into desired zebrafish embryos. By this method, the Tol2 element with the desired *QUAS-switchGFPcaax* construct is integrated into the genome.

2.2.2. The CRISPR Cas9 knock-in method

This project also requires labelling of RGCs expressing two TFs to target the various larval clusters related to LC13. For example, *eomesa*+ *onecut1*+ RGCs are to be labeled to target LC4. To narrow down the labeling from RGCs expressing a particular TF to RGCs expressing two particular TFs, the intersectional principle (Section 2.1.3) is

coupled with the CRISPR Cas9 knock-in approach to create appropriate Cre lines for this project. For example, this approach would help generate transgenic lines of genotype *onecut1:Cre eomesa:QF2 QUAS:switchGFPcaax* which will label all *eomesa+* cells red and only *eomesa+ onecut1+* cells green.

The CRISPR (Clustered Regularly Interspaced Palindromic Repeats) technique of gene editing has two components: the Cas9 (CRISPR associated protein) endonuclease and the guide RNA. The guide RNA, gRNA, is a RNA duplex made up of a trans-activating RNA (tracrRNA) essential for binding Cas9 and the sequence specific CRISPR RNA (crRNA). It is complementary to a specific DNA sequence and therefore, guides the Cas9 protein to these specific genomic regions. The Cas9 protein is an endonuclease that induces double stranded DNA breaks at these sites. The DNA repair that follows could either be non-homologous end joining (NHEJ) or homology-directed repair (HDR). NHEJ achieves DNA repair through deletions or insertions of sequences in the absence of a template while HDR uses a template with homology to the targeted locus to achieve DNA repair.[59]

To generate Cre lines, the HDR mediated CRISPR-Cas9 knock-in method is used. The constructs for HDR mediated insertion, *onecut1-Cre* and *opn4b-Cre* constructs, are generated using Gateway cloning methods (Section 2.2.3). They are homologous to the very short regions of *onecut1* and *opn4b* genes in the genome flanking the CrispR/Cas9 sites of selection, respectively. This construct is co-injected with the tracrRNA, crRNA and the Cas9 protein into the desired fertilized eggs, for eg. eggs resulting from in-crosses between transgenic fish expressing *eomesa:QF2 QUAS:switchNTR-tagRFP*, to induce HDR mediated insertion of the *onecut1-Cre* construct into the genome. This enables the labeling of *onecut1+ eomesa+* RGCs to target LC4 and *opn4b+ eomesa+* RGCs to target LC26 (Table 1). Similar strategy can be applied to label other LC13 related RGCs as well.

2.2.3. Golden gate assembly

The Golden Gateway Cloning methods are used to produce transgenic constructs used for the CRISPR-Cas9 mediated knockin approach. The entry vectors used for assembly in the destination vector, pGGDest, are:

Entry Vectors (EVs)	For opn4b	For onecut1
pGGEV1	Linker	Linker
pGGEV2	5’ HA-opn4b-GW-UgRNA	5’ HA-onecut1-GW-UgRNA
pGGEV3	GSG-linker-T2A	GSG-linker-T2A
pGGEV4	cre-SV40 polyA	cre-SV40 polyA
pGGEV5	cmlc2-GFP (coldheart)	cmlc2-GFP (coldheart)
pGGEV6	3’ HA-opn4b-GW-UgRNA	3’ HA-onecut1-GW-UgRNA

Table 2: List of entry vectors for producing transgenic constructs of *opn4b-Cre* and *onecut1-Cre.*

On cloning, all the six empty vector elements are integrated into a final plasmid vector. This plasmid vector is transformed into E.coli DH5α and extracted using midiprep. The plasmid vector is sequenced and used for microinjections (Section 2.3.3) later. This was done with Irene Arnold-Ammer (Baier Lab).

2.3. Zebrafish handling

2.3.1. Zebrafish maintenance

Zebrafish are maintained in the fish facility at the standard conditions of 14/10 hours day/night cycle at 28°C. The embryos are maintained in Daniaeu's buffer (pH 7.6, 17 mM NaCl, 1.8 mM $Ca(NO3)_2$, 2 mM KCl, 1.5 mM HEPES, 0.12 mM MgSO4) until seven days post fertilization (dpf) and raised in the fish facility afterwards. If the larvae are to be imaged in the retina, they are maintained in 0.2 mM phenylthiourea (PTU), which inhibits melanogenesisfrom 24 hpf. The zebrafish used in this report are six dpf, seven dpf and 21 dpf old.

2.3.2. Transgenic lines

The transgenic lines used in this project are given in Table 3:

Transgenic lines	**Reference**
ath5:Cre	Foerster et al, 2017
eomesa:QF2	Kölsch et al, 2021
onecut1:QF2	Baier Lab (unpublished)
tbx20:Gal4	Foerster et al, 2017
QUAS:switch-epNTR-tagRFP	Kölsch et al, 2021
QUAS:tagRFP	Kölsch et al, 2021
UAS:Dendra	Arrenberg et al, 2009

Table 3: Transgenic lines used.

2.3.3. Microinjections

Eggs of desired genotype are mounted on 2% agarose molds and injected with freshly prepared solutions of the transgenic constructs (about 2-3 nL).

For sparse labeling of *eomesa+* RGCs, *ath5:Cre eomesa:QF2 QUAS:tagRFP* eggs are injected with eight ng/uL Tol2-plasmid containing the construct *QUAS:switchGFPcaax*

along with 50 ng/uL Tol2 mRNA (Fig. 12). The concentration of the Tol2-plasmid is used such that as few eomesa+ RGCs are labelled as possible, preferably only a single one per eye.

For creating transgenic lines with *onecut1+ eomesa+* RGCs and *eomesa+ opn4b+* RGCs labeled, a CRISPR-Cas9 mediated knockin approach is used. Equimolar ratio of tracrRNA and target specific crRNA (one specific for *onecut1* or *opn4b* and the other for UgRNA sites of the plasmid) are annealed in a nuclease free buffer to form the gRNAs (guide RNAs). An equimolar concentration of Cas9 in the Cas9 working buffer is prepared. The gRNAs and Cas9 protein in 1:1 ratio are kept for 15 mins in 37°C to form the RNA-protein complex at 1.5 µM concentration. The donor plasmid containing the transgenic construct (*pGGEV2:Cre:coldheart: pGGEV6*) is added to this solution to a final concentration of 50 ng/µL. This solution is then injected into *eomesa:QF2 QUAS:switchNTR-tagRFP* eggs. This was done with Eva Laurell.

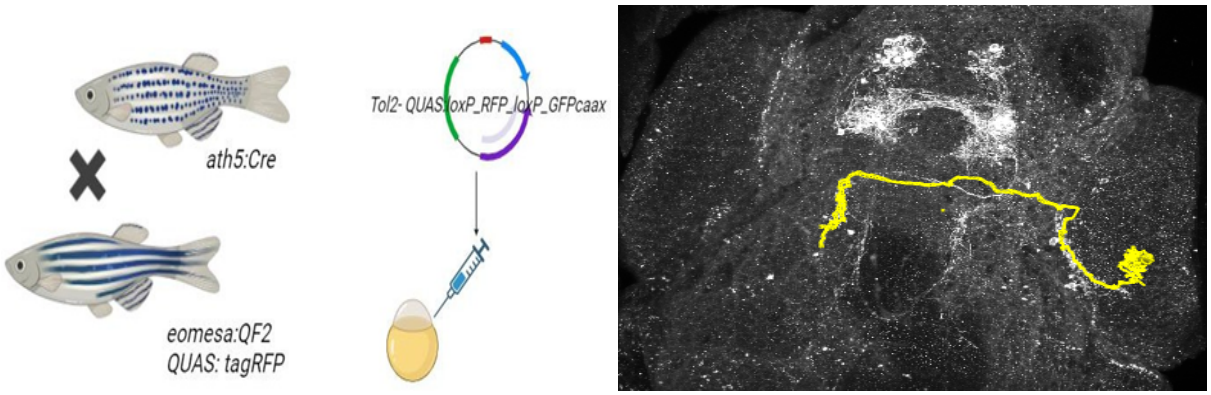

Fig. 12: Methodology for sparse labelling *eomesa+* RGCs: (A) Depiction of microinjections. (B) Tracing of a retinal ganglion cell from eye to optic tectum using neutube.

2.3.4. Chemogenetic ablation

To test the role of different RGC subtypes for specific behavior, the RGCs of interest were chemically ablated and then the fish were tested in a behavioral assay. The larvae of the desired genotype expressing the NTR enzyme in specific RGCs are sorted based on the reporters they express. For this project, larvae of genotype *ath5:Cre eomesa: QF2 QUAS:switchNTR* and *ath5:Cre onecut1:QF2 QUAS:switchNTR* are used. At five

dpf, they are administered with 2 mM ronidazole for 16 hours and given a recovery time of 24 hours in Daniaeu's buffer. The ablation is validated by confocal imaging of live fish mounted in 2% low melting agarose with a 20X water objective on Zeiss LSM700. This validation shows that the chemogenetic ablation with 2 mM Ronidazole on NTR expressing *eomesa*+ RGCs (Fig.14A and 14B) and *onecut1*+ RGCs (Fig.14C and 14D) were successful as no axons of the RGCs were found in the brain post ablation.

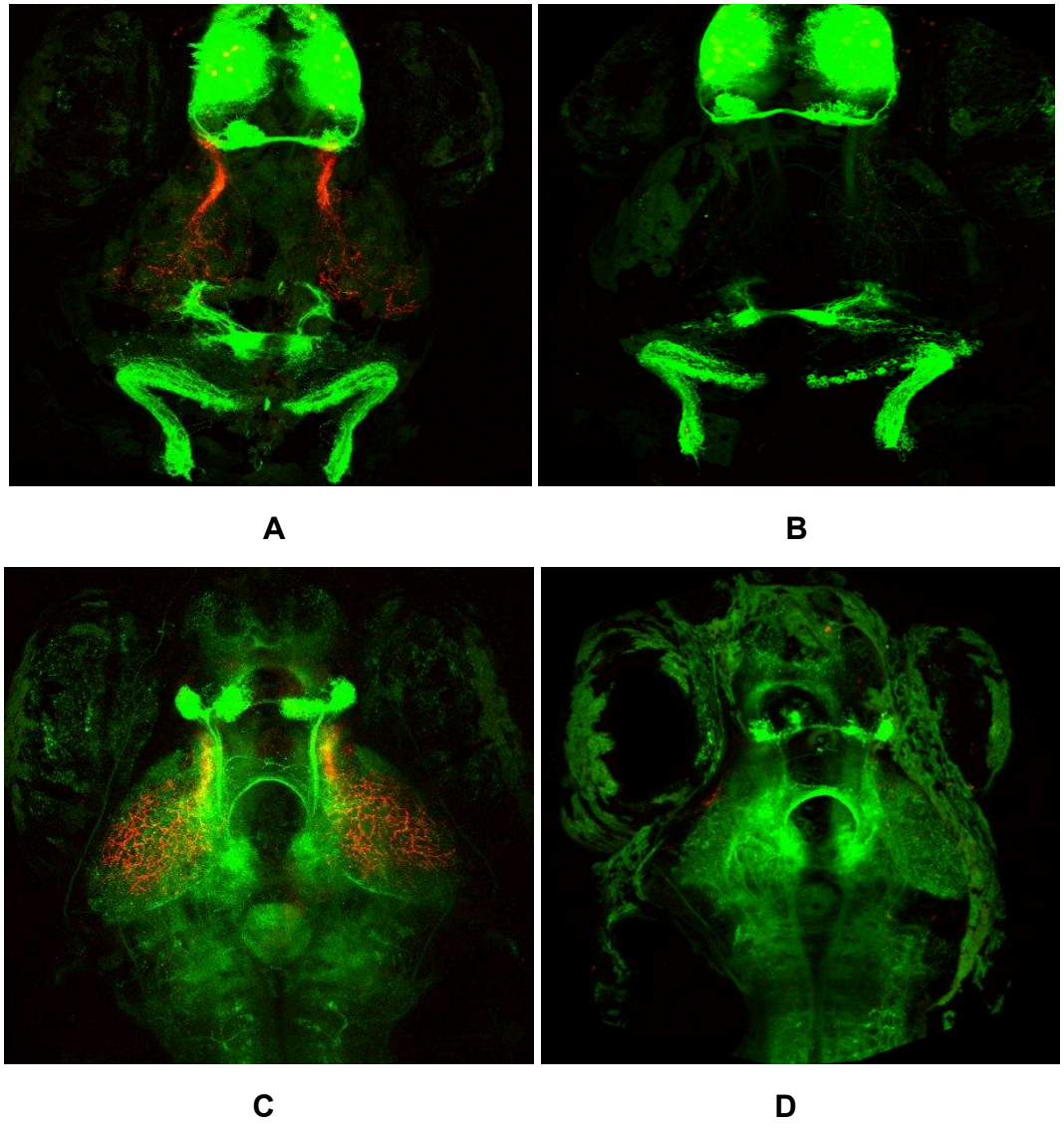

Fig. 14: *ath5:Cre eomesa:QF2 QUAS:switch-epNTR-tagRFP* fish treated with (A) 0.1% DMSO and (B) 2 mM Ronidazole in 0.1% DMSO for 16 hours and subjected to 24 hours recovery. *ath5:Cre onecut1:QF2 QUAS:switch-epNTR-tagRFP* fish treated with (C) 0.1% DMSO and (D) 2 mM Ronidazole in 0.1% DMSO for 16 hours and subjected to 24 hours recovery. Green depicts eomesa+ and onecut1+ cells while red depicts eomesa+ and onecut1+ RGCs.

2.4. Molecular biology techniques

2.4.1. Immunostaining fixed fish

To enhance and identify the morphology of sparsely labelled *eomesa*+ RGCs, immunostaining is performed on GFP labelled *eomesa*+ RGCs post microinjections. At the desired ages of six dpf and 21 dpf, the larvae and juveniles are euthanized with lethal doses of tricane for 5 mins and fixed in ice-cold PACT hydrogel monomer solution (4% acrylamide, 0.25% VA-044 initiator, 1x PBS, 4% PFA) at 4°C overnight. The hydrogel solution with the fish is polymerized at 37°C for at least three hours. The fish are then cleared using a clearing solution (pH 8.5, 4% SDS, 200 mM boric acid) for 48 hours (for larvae) and two weeks (for juveniles) and washed with PBT before staining. The juveniles are then bleached in a bleaching solution (1% H2O2, 1% KOH in Danieu buffer) for 15 mins to remove pigmentation in the eye. This step is necessary to image the juveniles as they are not raised with PTU. Trypsin digestion is done in cold trypsin-EDTA (1:20 for larvae and 1:10 for juveniles) on ice for 45 minutes followed by thorough washing with PBT. Blocking solution (5% goat serum, 1% BSA, 1% DMSO in PBT) is then administered to the fish for two hours before incubating them in primary antibodies (Invitrogen anti-GFP chicken IgY fraction (unconjugated) and Cell Signalling Technology p44/42 MAPK (Erk1/2) L34F12 Mouse mAb, 1:250 each) at 4°C for three days (for larvae) and one week (for juveniles). The fish are washed and incubated in secondary antibodies (Alexa-488 anti-chicken and Alexa-647 anti-mouse, 1:250 each) at 4°C for three days (for larvae) and one week (for juveniles). The fish are then post-fixed in 4% PFA and stored in 87% glycerol at 4°C. The larvae and juveniles are mounted in glycerol for imaging. The immunostaining procedure for fixed juveniles and adults can also be performed on dissected retina. The retina is then flatmounted using mounting media for imaging. The confocal images are obtained using a 25X glycerol objective on Zeiss LSM700 and Zeiss LSM900. Image analysis is done in ImageJ and semi-automatic tracing of the labelled RGCs is done in neutube.

2.4.2. *In situ* hybridization chain reaction (HCR)

In situ hybridization chain reaction (HCR) is used to image mRNA expression in cells using a DNA amplification technique. DNA probes specific to desired mRNA targets and potentially fluorescent metastable DNA hairpins are two essential substrates for this procedure. The DNA probes bind the desired mRNA target using the complementary probe sequences and bind the hairpin 1 (H1) using the initiator sequences. H1 is opened up to hybridize with hairpin 2 (H2) due to their complementarity. This cascade releases the kinetically trapped DNA hairpins to form tethered fluorescent amplification polymers. Thus, the cells that express the desired mRNA are labelled fluorescent. (Fig. 13). [60]

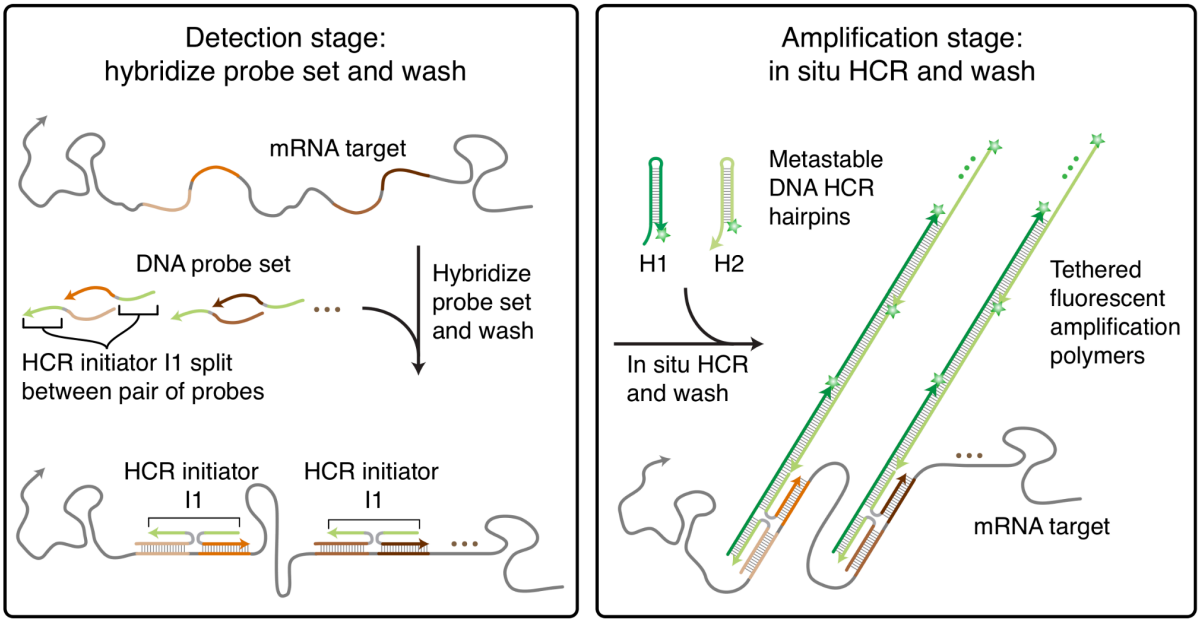

Fig. 13: HCR mechanism, Choi et al (2018)[60].

After the microinjections for sparse labelling of *eomesa*+ RGCs, 1-10, six dpf larvae are fixed in 1 mL of fresh 4% PFA in 1X DPBS (PBS without MgCl2 and CaCl2) at 4°C for 24 hours. The larvae are washed three times with DPBS-T (0.1% Tween-20 in 1X DPBS) for five mins each to stop the fixation. They are then permeabilized for 10 mins with cold 100% methanol kept in -20°C. This is followed by five minute washes with 50% and 25% methanol in DPBS-T. The larvae are pre-hybridized with 500 µL of probe hybridization buffer for 30 mins in 37°C. They are then incubated in 500 µL of probe

solution (2 pmol of each probe set) at 37°C for 12-16 hours. For this project, probes corresponding to *onecut1, eomesa, tbx20, opn4b* and *opn4xa* were used. The larvae are washed with 500 µL of probe wash buffer four times for 15 mins each at 37°C to remove excess probes. The larvae are then washed in 5X SSC-T (0.06 M sodium citrate, 0.6 M NaCl, 0.1% Tween-20) twice for 5 mins each at room temperature before administering them to pre-amplification with 500 µL of amplification buffer for 30 mins at room temperature. A hairpin solution is prepared by snap cooling (incubate at 95°C for 90 secs and cool at room temperature in a dark space for 30 mins) 30 pmol of hairpin 1 and 30 pmol of hairpin 2 of the same fluorescent wavelength. The larvae are incubated in hairpin solution in the dark at room temperature for 12-16 hours. The excess hairpins are washed with 500 µL of 5X SSC-T three times for 20 mins at room temperature.

2.4.3. Gold RNA-fluorescence *in-situ* hybridization (RNA-FISH)

To enhance the signal from *in-situ* HCRs, a modified protocol called Gold RNA-FISH is used. All the buffers and antibodies used are from the HCR™ Gold RNA-FISH kit (Molecular Instruments). After the microinjections for sparse labelling of *eomesa+* RGCs, 1-10 six dpf larvae are fixed in 1 mL of fresh 4% PFA in 1X DPBS for 24 hours at 4°C. The larvae are washed thrice with 1X DPBS-T for five mins each to stop the fixation. They are then kept in cold trypsin-EDTA (1:20) on ice for 45 minutes followed by thorough washing with DPBS-T. The samples are blocked with 500 µL of Antibody Buffer for 4 hours at room temperature. Following overnight incubation with working concentrations of the primary antibody in Antibody Buffer, the larvae are washed with DPBST at room temperature four times for 30 mins each. One µg/mL of secondary antibody in Antibody Buffer is administered to the larvae for 3 hours at room temperature. The excess antibodies are removed by washing the samples five times for five mins each with 500 µL 1X DPBST at room temperature. They are post-fixed with 4% PFA at room temperature for 10 mins. The fixative is removed by washing the samples twice with 500 µL 1X DPBST. Following this, the HCR protocol (Section 2.4.2) is followed by the probe hybridization step.

2.5. Behavioral assays

2.5.1. Phototaxis assay

To study the phototactic abilities of larval zebrafish, a closed-loop phototaxis assay is performed post chemogenetic ablation (Section 2.3.4). The larvae are placed in Daniaeu's buffer in a circular compartment made of 4% agarose in a petri dish and covered with a glass coverslip. They are then placed in the holder of the light-dark arena (Fig. 15) to test their preference to turn towards light as a measure of phototaxis. White light is projected onto the fish by a 240 Hz projector as visual stimuli. IR light is projected onto the fish by the IR lamp for tracking the fish. The camera placed beneath the holder acquires images at 100 frames per second. The fish is exposed to bright light for acclimatization for 300 seconds. The camera and the projector coordinate to expose white light to only one side of the fish for the next 300 seconds. This polarity is changed after 300 seconds. (Protocol in Fig.15).The data obtained is subjected to principal component analysis (PCA). The position of the fish in the dish is linearly transformed onto a new coordinate system with coordinates capturing the maximum variability. Subjecting these coordinates to a tan inverse function gives the angle of the fish so that a cumulative angle vs time graph can be plotted. If the slope of this graph is positive, it means the fish is turning anti-clockwise towards left while a negative slope means the fish is turning clockwise towards right. The python code for plotting these graphs was coded by Martin Privat (Baier Lab).

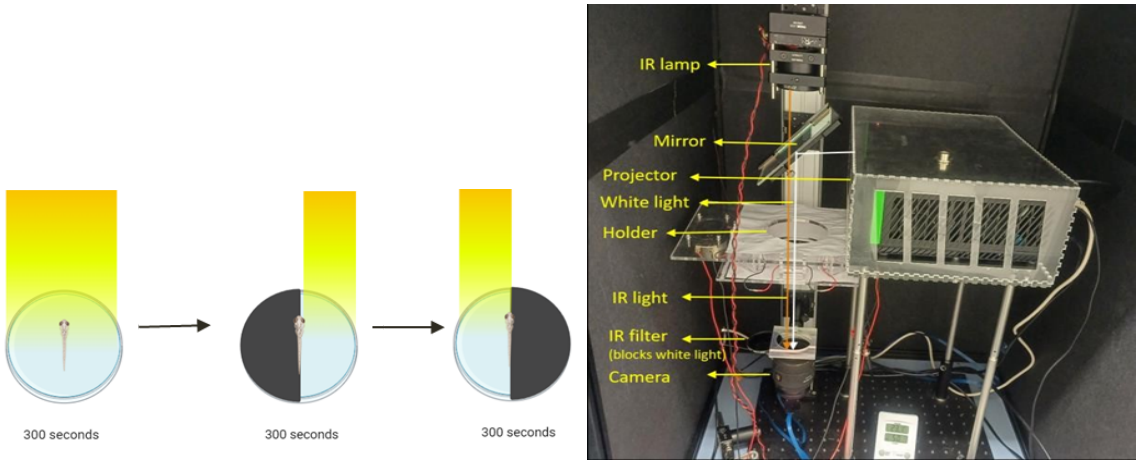

Fig. 15: (A) Phototaxis assay protocol. (B) Phototaxis assay apparatus set up by Martin Privat (Baier Lab).

Chapter 3: Results and Discussion

3.1. Characterization of *eomesa*+ RGCs morphology over time

3.1.1. Single *eomesa*+ RGCs are traced to identify their morphology.

To understand the development of RGC subtypes over time, matching the different *eomesa*+ RGC transcriptomic types to their morphology is crucial. As the first step to achieving this, the main objective of this project is to create a catalogue of *eomesa*+ RGC morphotypes in different developmental stages, i.e, larvae and juveniles. For this purpose, sparse labeling of *eomesa*+ RGCs were done to characterize their dendritic and axonal morphology. To label *eomesa*+ RGCs sparsely, microinjections of the *QUAS:switchGFP* construct on the eggs of *ath5:Cre eomesa:QF2 QUAS:tagRFP* were performed. The six dpf larvae of genotype *ath5:Cre eomesa:QF2 QUAS:switchGFP* were fixed and immunostained for GFP. This is then followed by probing for single *eomesa*+ RGCs labelled with GFP and imaging them using a confocal microscope. The images were then semi-automatically traced using the neutube software and loaded onto the mapZebrain atlas[64], a multimodal atlas of the brain of zebrafish larvae, to identify their dendritic structure and axonal projection pattern. (Fig. 16).

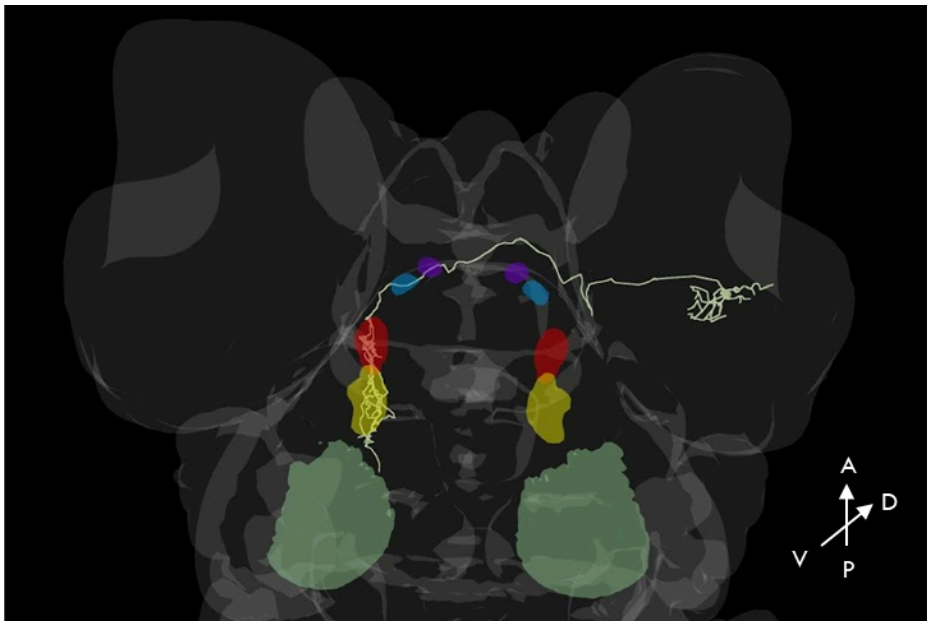

Fig.16. Trace of single *eomesa*+ RGC. Ventral view of the brain showing tectum (light green), AF9 (yellow), AF4 (red), AF2 (blue) and AF1 (purple). Orientation: A, Anterior; P, Posterior; D,Dorsal; V, Ventral. Diffuse RGC innervating AF4 and AF9 is shown in white.

3.1.2. Seven different morphotypes of *eomesa*+ RGCs were found based on dendritic stratification in six dpf old zebrafish larvae

To catalogue the *eomesa*+ RGC morphotypes based on dendritic stratification, imaging of about 120 single *eomesa*+ RGCs was done using the methodology described in section 3.1.1. This revealed the presence of seven different morphotypes based on dendritic stratification. This includes three monostratified: Mono1, Mono3 and Mono4, two bistratified: Bi1 and Bi3 and two diffuse: Diff1 and Diff2 dendritic morphologies.

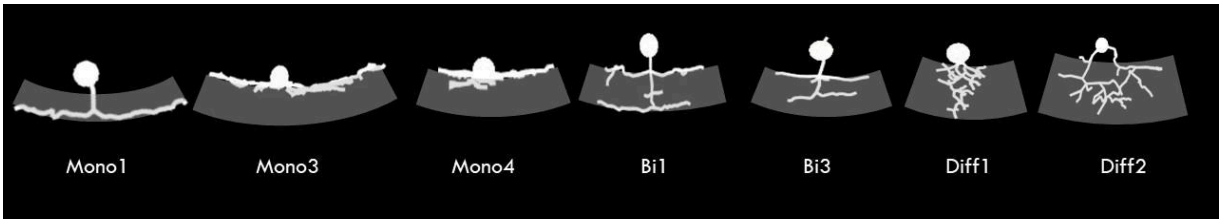

Fig. 17: The seven different dendritic morphologies of *eomesa*+ RGCs in 6 dpf old zebrafish larvae. RGCs are depicted in white while the IPL boundaries are in grey.

As the name suggests, the monostratified dendrites extend into only one layer of the IPL. The monostratified subtypes are classified based on which layer of the IPL they innervate. Mono1 targets the OFF layer of the IPL, S1, while Mono3 and Mono4 target the ON layer of the IPL, S5. Mono4 subtypes extend filopodia-like structure into other layers of the IPL while Mono3 do not. About 40% of the *eomesa*+ RGCs found were of monostratified morphotypes, Mono3 and Mono4, making them the most abundant. This implies that the majority of the *eomesa*+ RGCs are monostratified, extending their dendrites into the ON layer of the IPL. The second most common morphotypes are those of diffuse dendritic stratification, Diff1 and Diff2, making about 30% of the *eomesa*+ RGCs. Both the diffused dendritic morphotypes lack structured stratifications in the IPL. The Diff1 types that arborize throughout the IPL contribute to about 88% of the diffuse dendrites while a minor fraction of 12% consists of Diff2 types with arborizations in between S3 to S5. of the IPL. A significant population of about 25% of the RGCs are also bistratified. The bistratified types, Bi1, arborizes in layers S1 and S5 and contributes to 36% of the bistratified RGCs. The remaining bistratified RGCs are of Bi3 type that arborizes in S1 and S3. Interestingly, monostratified RGCs of type Mono1, which extend into the OFF layer, were found very rarely contributing to about 3% of the RGCs. (Table 4).

Type	Subtype	Image	Number	Percentage
Monostratified	Mono1	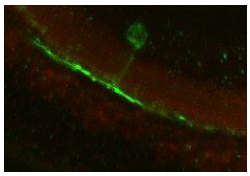	4	3.33
	Mono3	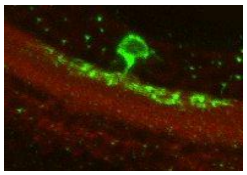	41	34.17
	Mono4	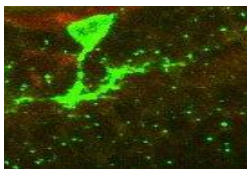	9	7.5
Bistratified	Bi1	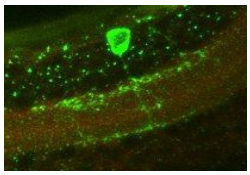	11	9.17
	Bi3	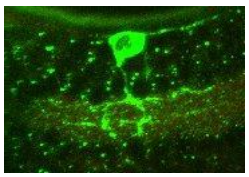	19	15.83
Diffuse	Diff1	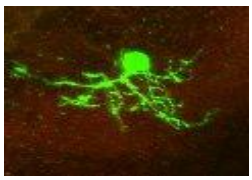	32	26.67
	Diff2	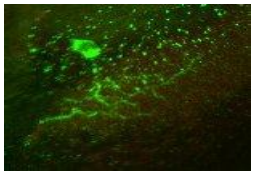	4	3.33

Table 4: Table showing confocal images of the different *eomesa*+ RGCs morphotype with their abundance given in number and percentage in 6 dpf old zebrafish larvae. The *eomesa*+ RGCs are stained with anti-GFP antibodies (green) while the background is stained with anti-p44/42 MAPK (Erk1/2) antibody (red) indicating the IPL boundaries.

3.1.3. Seven different morphotypes of *eomesa*+ RGCs were found based on axonal projection patterns in 6 dpf old zebrafish larvae

Complete information on the morphology of RGCs is defined by both the stratification of their dendritic stratification pattern and the regions innervated by their axons, i.e, axonal projection pattern. To decode the axonal projection pattern of RGCs, their axons were traced using neutube post confocal imaging and the traces were overlapped to the zebrafish larval brain in the mapZebrain atlas to identify the regions arborized by these axons.

On tracing the axons of sparsely labelled *eomesa*+ RGCs, seven different projection patterns were found (Table 5). Almost all the RGCs innervate AF9 and terminate in SAC and form five projection classes: AF1, AF4 (PC1); AF2, AF4 (PC2); AF1, AF2, AF4 (PC3); AF1, AF3 (PC4); AF4 (PC5). Few RGCs also innervate AF4 and terminate in AF9 (PC6). Rarely, some RGC axons only arborize in deeper layers of the tectum like SFGS (PC7).

Projection class (PC)	Regions innervated
PC1	AF1, AF4, AF9, SAC
PC2	AF2, AF9, SAC
PC3	AF1, AF2, AF4, AF9, SAC
PC4	AF1, AF3, AF4, AF9, SAC
PC5	AF4, AF9, SAC
PC6	AF4, AF9
PC7	SFGS

Table 5: Seven different projection classes of eomesa+ RGCs in six dpf old zebrafish larvae.

In addition to the PCs identified by Robles et al (2014)[2], PC1 and PC4 were identified. PC1 RGCs innervate AF1, AF4, AF9 and SAC while PC4 RGCs innervate AF1, AF3,

AF4, AF9 and SAC. The other observed PCs could be correlated to the PCs found in Robles et al (2014): PC2 to PC18, PC3 to PC19, PC5 to PC17, PC6 to PC15 and PC7 to PC3. Many axonal projection patterns correspond to a single dendritic stratification leading to 12 different morphological types of *eomesa*+ RGCs (Fig.18).

RGCs with monostratified dendrites innervating the ON layer, Mono3 and Mono4, correspond to six projection classes: PC1, PC2, PC3, PC4, PC5 and PC6 (Fig.19A). The RGCs with bistratified dendrites, Bi1 correspond to two different projection classes: PC1 (Fig.19B) and PC5. Interestingly, in addition to PC5, RGCs with Bi3 dendrites also correspond to the unique PC7 innervating a SFGS sublayer of the tectum as opposed to others that mostly terminate in the SAC sublayer. RGCs with diffuse Diff1 dendrites correspond to PC3 while those with Diff2 dendrites interestingly terminate in AF9 (PC6) instead of SAC (Fig.19C). The rare M1 monostratified RGCs follow the PC1 projection pattern and project to AF1, AF4, AF9 and SAC. (Fig.18).

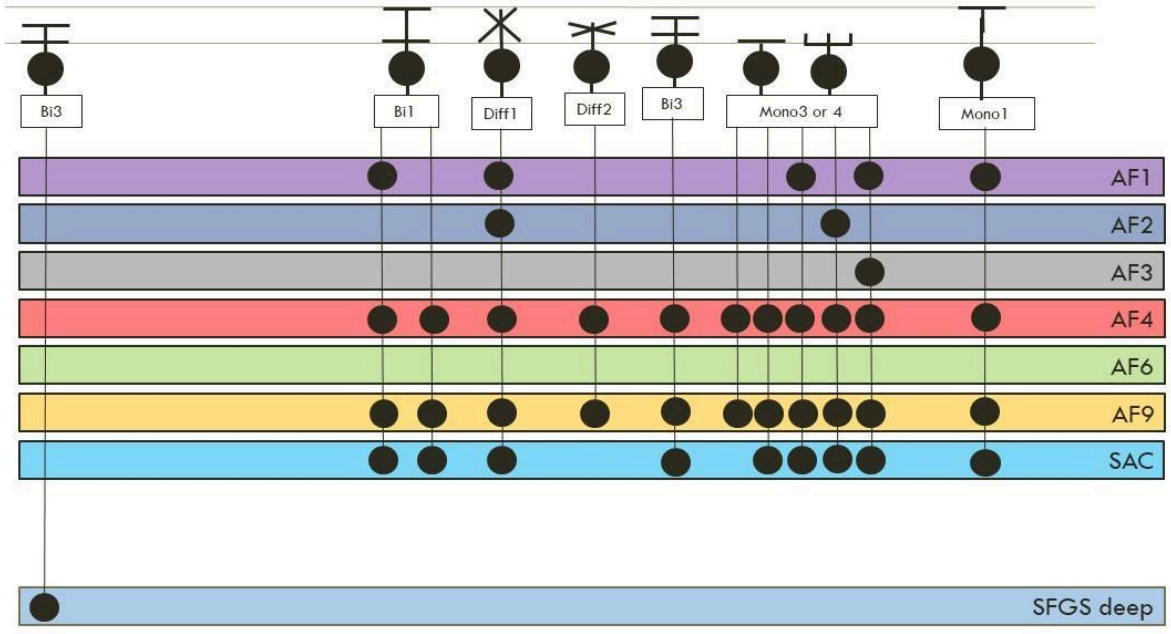

Fig. 18: The 12 different morphologies of *eomesa*+ RGCs observed in six dpf old zebrafish larvae based on dendritic stratification and axonal projection classes.

Since almost all *eomesa*+ RGCs project to and some even stop at AF9, this correlation might have interesting functional implications. Optomotor responses are reflexive

responses shown by zebrafish to stabilize themselves in response to optic flow like grating motion, i.e, flow of bright and dark stripes alternatively. Semmelhack et al (2014)[61], suggests that laser ablation of AF9 results in reduction in optomotor responses to grating motion. Kubo et al (2014)[62] also shows optogenetic activation of AF9 led to optokinetic eye movements. However, recent developments[63], suggest that this could be because of the ablation of the region ventral to AF9, i.e, AF5. In Kölsch et al (2021)[1], it was shown that ablation of eomesa+ RGCs did not affect optomotor response, escape behavior or overall locomotor activity. From what is known so far, the neural circuit involving *eomesa*+ RGCs is not involved in optomotor responses despite its connections in AF9.

Note: The catalogue of eomesa+ RGC morphotypes in 6 dpf is in preparation to be submitted as part of a publication

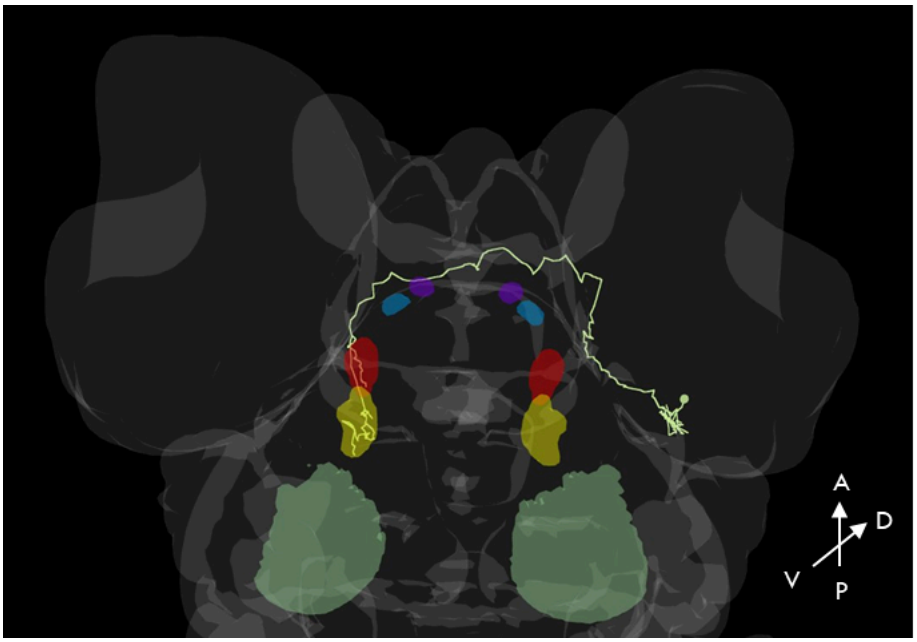

A

B

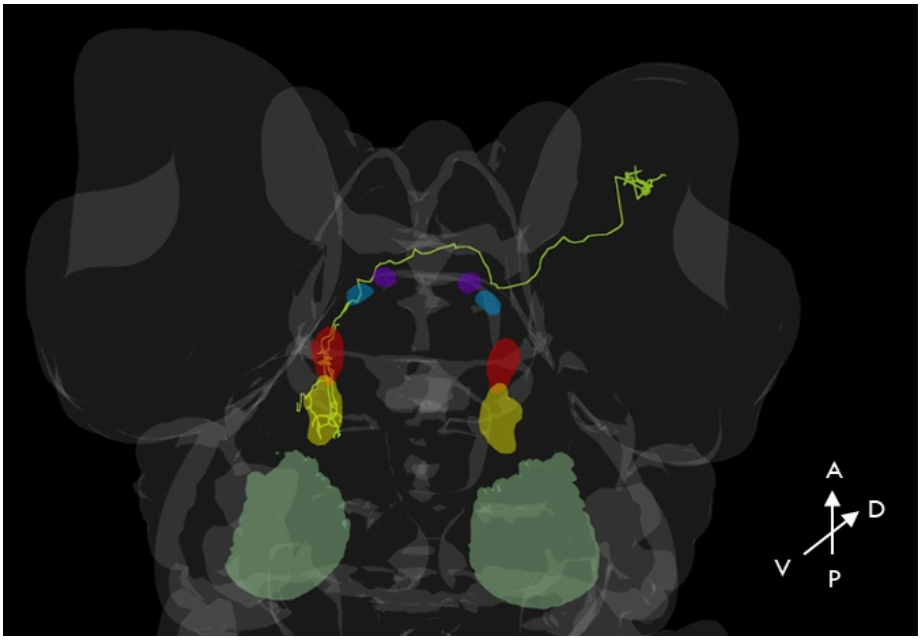

C

Fig.19: Ventral view of the brain showing tectum (light green), AF9 (yellow), AF4 (red), AF2 (blue) and AF1 (purple). Orientation: A, Anterior; P, Posterior; D,Dorsal; V, Ventral. (A) Monostratified RGC (white) innervating AF4 and AF9. (B) Bistratified RGC (pink) innervating AF1, AF4, AF9, SAC. (C) Diffused RGCs (green) innervating AF4 and AF9. Images generated in mapzebrain atlas.[64]

3.1.4. Mono1 *eomesa*+ RGCs in zebrafish show similarities to M1 ipRGCs in mice

In six dpf old larvae, monostratified RGCs of type Mono1, which extend into the OFF layer, were found contributing to about 3% of the RGCs. This reveals an interesting morphological correlation between *eomesa*+ RGCs in zebrafish and intrinsically photosensitive RGCs (ipRGCs) in mice. It is assumed that *eomesa*+ RGCs in zebrafish are ipRGCs due to their transcriptomic and functional similarities with mice ipRGCs. Both *eomesa*+ RGCs in zebrafish and ipRGCs in mice express *eomesa/Tbr2* and opsins[1][46]. *eomesa*+ RGCs are involved in non-image forming functions like phototaxis[1] in zebrafish larvae while ipRGCs in mice are known to be involved in non-image forming functions like maintenance of the circadian rhythm[39].

The zebrafish Mono1 *eomesa*+ RGCs follow the PC1 projection pattern and project to AF1, AF4, AF9 and SAC. This projection pattern is interesting as AF1 is implied in circadian rhythm regulation[30]. In mice, M1 is an important subtype of ipRGCs innervating the OFF layer of the IPL and projecting directly to different non-image forming centers of the brain executing different functions. For example, the suprachiasmatic nucleus (SCN) involved in circadian rhythm receives inputs from M1 to a larger extent compared to M2, the ON layer monostratified ipRGC.[65][66] These connections can lead to an interesting hypothesis highlighting the functional relevance of Mono1 *eomesa*+ RGCs in circadian rhythm in zebrafish.

3.1.5. Five different morphotypes of eomesa+ RGCs were found based on dendritic stratification in 21 dpf old zebrafish

On comparing the transcriptomic *eomesa*+ RGC types between larval and adult stages of zebrafish, Kölsch et al (2021)[1] showed significant change in the transcriptomic population of *eomesa*+ RGCs over time. Five *eomesa*+ RGC clusters were found in larvae while only three remain in the adult. This could be because of refinement and removal of certain RGC types over the course of development. It is intriguing to study the morphological reflection of this aspect by documenting the changes in *eomesa*+ RGC morphotypes over time. To achieve this, the sparse labelling technique was also

used on three week old zebrafish juveniles to catalogue the RGC morphotypes and to compare them with six dpf old larvae.

The analysis of the dendritic morphology of 21 single RGCs revealed five different morphotypes of *eomesa*+ RGCs. Dendrites with monostratified: Mono3 and Mono4, bistratified: Bi1 and diffuse: Diff1 and Diff2 stratification patterns were observed (Fig.20).

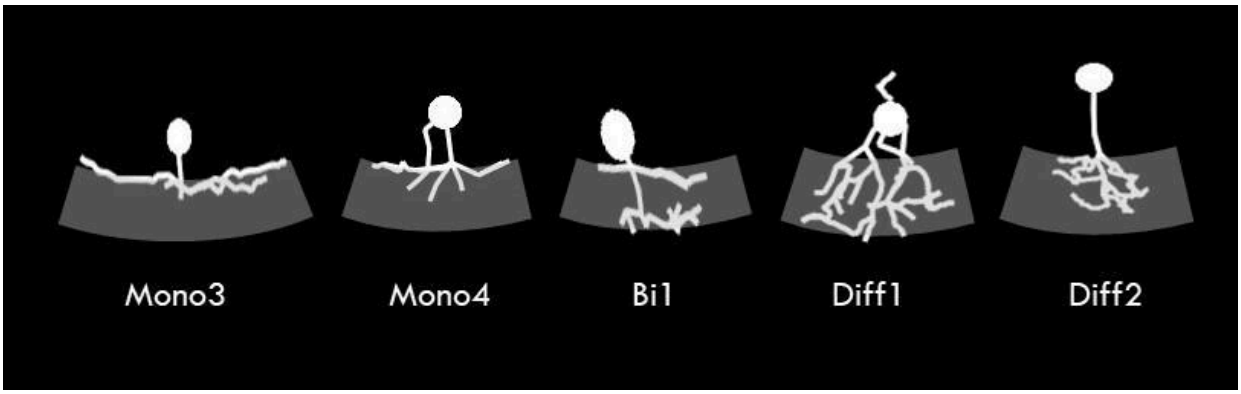

Fig. 20: The five different dendritic morphologies of *eomesa*+ RGCs in three week old zebrafish juveniles.RGCs are depicted in white while the IPL boundaries are in grey.

From Table 4, it is clear that about 50% of the RGCs have monostratified dendrites: Mono3 and Mono4. About 30% of the RGCs have diffused Diff1 and Diff2 dendrites while about 20% of the RGCs have bistratified, Bi1 dendrites. Overall, the catalogue of *eomesa*+ RGCs morphotypes in 21 dpf old juveniles showed high correspondence with that of six dpf old larvae.

Interestingly, Bi3 bistratified dendrites and Mono1 monostratified dendrites were not found in 21 dpf old zebrafish adults. However, to conclude that this is because they are lost over the course of development, more juveniles are to be analyzed for a statistically significant conclusion.

Type	Subtype	Image	Number	Percentage
Monostratified	Mono3	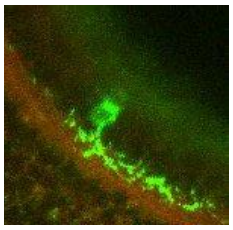	9	42.86
	Mono4	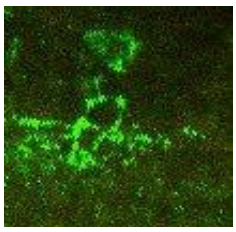	1	4.76
Bistratified	Bi1		4	19.05
Diffused	Diff1	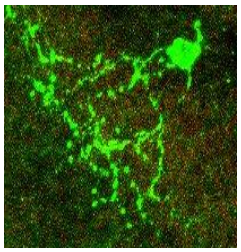	4	19.05
	Diff2	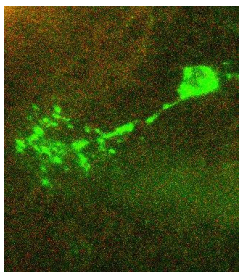	3	14.29

Table 6: Table showing confocal images of the different *eomesa*+ RGC morphotypes in three week old zebrafish juveniles with their abundance given in number and percentage. The *eomesa*+ RGCs are stained with anti-GFP antibody (green) while the background is stained with anti-p44/42 MAPK (Erk1/2) antibody (red) indicating the IPL boundaries.

3.1.6. The abundance of *eomesa*+ RGCs is reduced over the course of development

While the transcriptomic data from Kölsch et al (2021)[1] suggest that several *eomesa*+ RGC types are lost from larva to adult zebrafish, the population of *eomesa*+ RGC morphotypes showed high similarity between larval and juvenile stages. To understand if the loss of transcriptomic *eomesa*+ RGC types could be seen in the total number of eomesa+ RGCs, retinas from two different developmental stages of *eomesa:QF2 QUAS:loxP_GFP_loxP_tagRFP* fish: three week old juveniles and six month old adults were dissected and stained for GFP. The retinas were thereafter flat-mounted, imaged and compared with the confocal images of six dpf old larval retina. Interestingly, it was found that numbers of *eomesa*+ RGCs labelled with GFP are reduced in the case of juveniles and adults compared to larvae (Fig.21).

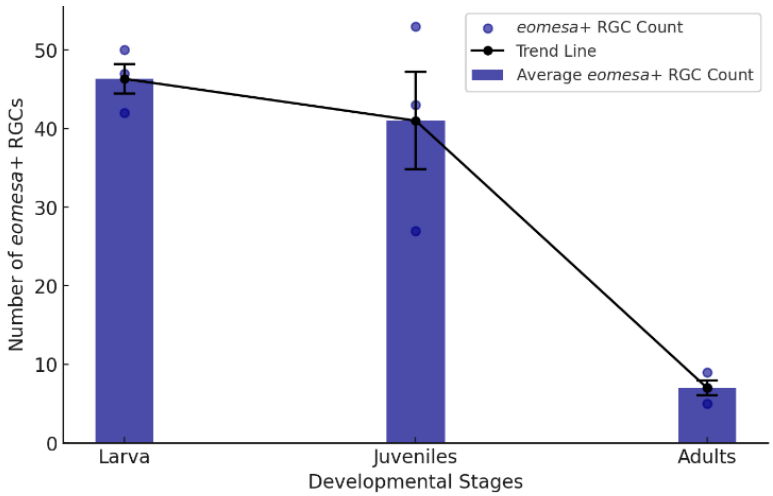

Fig. 21: The total number of *eomesa*+ RGCs from three different developmental stages, six dpf larvae, 21 dpf old juveniles and adults, of *eomesa:QF2 QUAS:loxP_GFP_loxP_tagRFP* fish are plotted with n=3 each.

According to Kölsch et al (2021)[1], the adult cluster, AdC24, is the most enriched in *eomesa*. In addition to eomesa, it also expresses *onecut1* and *tbx20*. To understand if this is the population of surviving *eomesa*+ RGCs in adults, retina dissected from six month old adult *tbx20:Gal4 UAS:Dendra* fish were imaged to compare them with those of *eomesa:QF2 QUAS:switch-tagRFP*. As expected, the numbers of *tbx20*+ RGCs were comparable to that of *eomesa*+ RGCs in adults, i.e, six RGCs with axons extending into

the optic tract were identified in retina from *tbx20: Gal4 UAS:Dendra* adults which is comparable to the average number of RGCs found in *eomesa:QF2 QUAS:switch-tagRFP* adults (Fig. S1). This suggests that the majority of the surviving *eomesa*+ RGCs could express *tbx20*. This also suggests that there could be refinement and removal of certain *eomesa*+ RGC types during development.

3.1.7. Mono3 and Mono4 morphotypes are the most abundant in *eomesa*+ RGCs

In Kölsch et al (2021)[1], the bioinformatic analysis of the larval transcriptional data showed that *eomesa* is mostly enriched in the larval cluster 4 (LC4) expressing *eomesa*, *onecut1* and *tbx20*. To understand the morphology of this cluster, RGCs of the *tbx20:Gal4 UAS:Dendra* fish with *tbx20*+ RGCs labelled with Dendra were imaged[1]. They were shown to have Mono3 monostratified dendrites and axonal projection pattern innervating AF4 and AF9 (PC6)[1].

In agreement with the transcriptomic data, our data showed that the most abundant *eomesa*+ RGCs in six dpf old larvae were monostratified with Mono3 and Mono4 dendrites (Section 3.1.1). This might suggest that Mono3 and Mono4 *eomesa*+ RGCs belong to LC4 and express *onecut1* and *tbx20*. However, RGCs with monostratified dendrites innervating the ON layer correspond to six different projection classes: PC1-PC6. Only, RGCs of the projection class, PC6, project to regions, AF4 and AF9 similar to the pattern shown by *tbx20*+ RGCs. This points to the fact that all the monostratified *eomesa*+ RGCs of type Mono3 and Mono4 with axonal projection classes PC1-PC5 (Section 3.1.3) do not express *tbx20*.

The abundance of monostratified dendrites, Mono3 and Mono4, is preserved in 21 dpf old juveniles (Section 3.1.5). Correlating the most abundant *eomesa*+ RGC morphotype with the adult cluster most enriched with *eomesa*, this monostratified population could belong to the AdC24. AdC24 corresponds to *eomesa, onecut1* and *tbx20* expressing LC4 which also contains monostratified RGCs. This could suggest that the morphology of the monostratified *eomesa*+ RGCs is preserved. Interestingly, the number of *eomesa*+ RGCs decrease with age with *tbx20*+ RGCs surviving in abundance. This could explain why AdC24 is the most dominant *eomesa* expressing RGC cluster in adults according to transcriptomics.

3.2. Correlating dendritic morphology to genetic expression using *in situ* hybridization chain reaction (HCR)

To better correlate the morphological *eomesa*+ RGC types with the transcriptomic types, we were interested in deciphering patterns of gene expression in *eomesa*+ RGCs of specific dendritic morphology. To achieve this, *in-situ* HCRs for various genes are performed on sparsely labelled *eomesa*+ RGCs at six dpf old larval stage.

Kölsch et al. (2021)[1] revealed that the *eomesa* expressing larval cells can be further characterized into subtypes or larval clusters based on their gene expression. Apart from *eomesa*, the precursor LC13 expresses *onecut1* and *tbx20*; LC4 expresses *onecut1, tbx20, opn4xa* and *opn4b*; LC18 expresses *opn4xa* and *opn4b*; LC26 expresses *opn4b* and LC19 expresses *onecut1*. To map the subtypes to their dendritic morphology, *in situ* HCRs are performed for *opn4xa, opn4b* and *onecut1* on labelled *eomesa*+ RGCs and for *eomesa* and *onecut1* on labelled *tbx20*+ RGCs.

3.2.1. *In-situ* HCRs for *opn4xa* and *opn4b* on *eomesa*+ RGCs revealed transcriptomic insights on LC13 related RGCs

To understand the dendritic morphology of *eomesa*+ RGCs that also express the opsins: *opn4xa* or *opn4b* or both, sparse labelling of *eomesa*+ RGCs was coupled with HCRs for *opn4xa* and *opn4b* in six dpf old zebrafish larvae. This led to the identification of *eomesa+ opn4xa+ opn4b+*, *eomesa+ opn4xa- opn4b+*, *eomesa+ opn4xa+ opn4b-* and *eomesa+ opn4xa- opn4b-* RGCs.

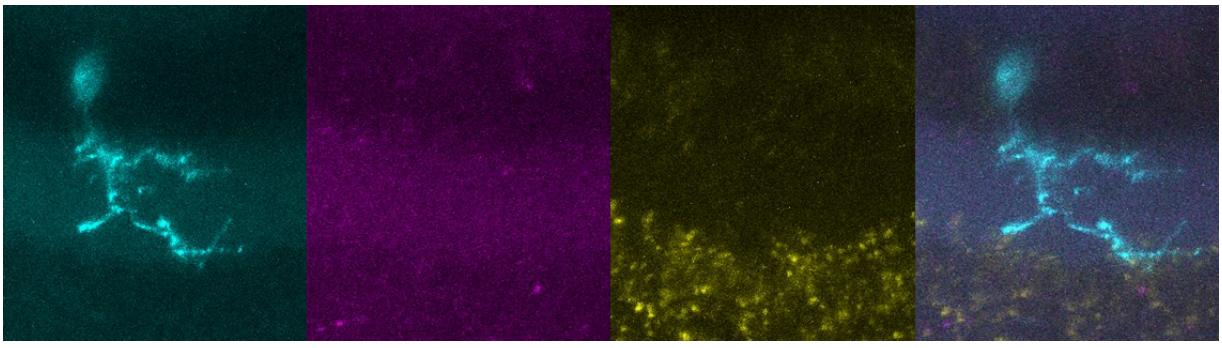

A **B** **C** **D**

Fig. 22: (D) Bistratified *eomesa*+ RGC labelled with GFP (A, cyan) not expressing *opn4xa* (B, magenta depicting the 546 nm HCR hairpin specific for *opn4xa*) and *opn4b* (C, yellow depicting the 647 nm HCR hairpin specific for *opn4b*).

Analysis of ten *eomesa*+ RGCs revealed monostratified (Mono3 and Mono4) and bistratified (Bi1 and Bi3) dendritic stratification. Interestingly, 100% of the bistratified *eomesa*+ RGCs of subtypes Bi1 and Bi3 do not express either of the opsins. This suggests that bistratified *eomesa*+ RGCs do not belong to the opsin containing RGCs. (Fig.22)

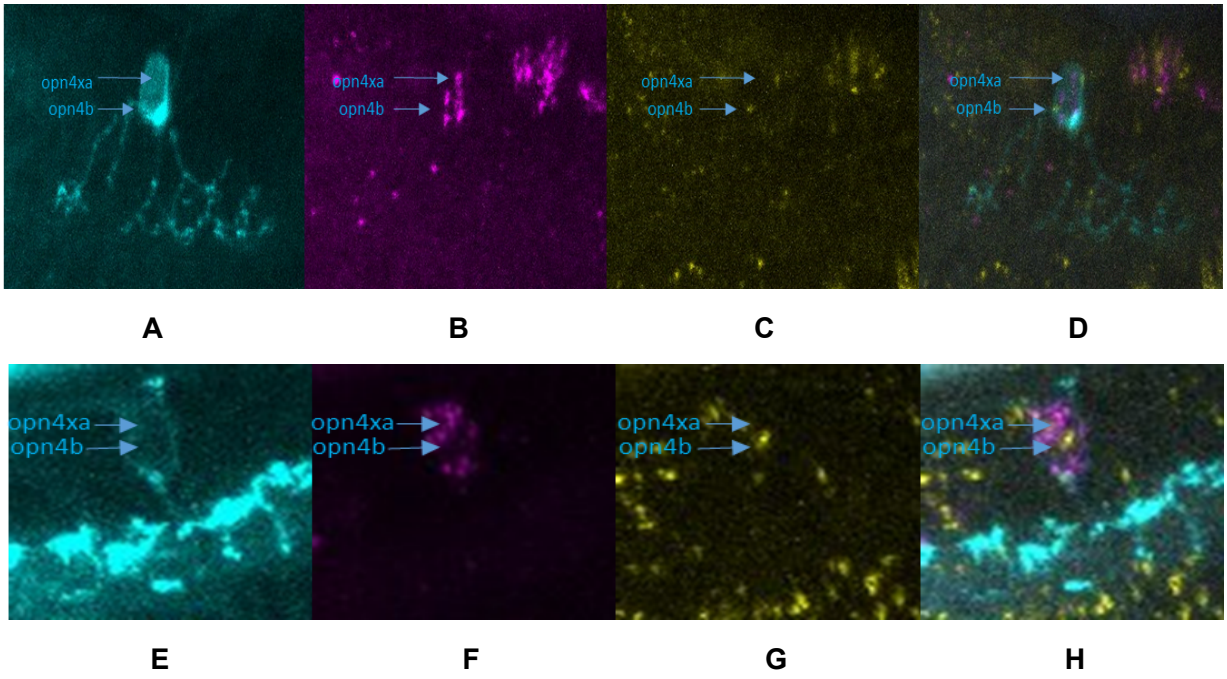

Fig.23: (D and H) Monostratified *eomesa*+ RGcs labelled with GFP (A and E, cyan) expressing both *opn4xa* (B and F, magenta depicting the 546 nm HCR hairpin specific for *opn4xa*) and *opn4b* (C and G, yellow depicting the 647 nm HCR hairpin specific for *opn4b*) respectively.

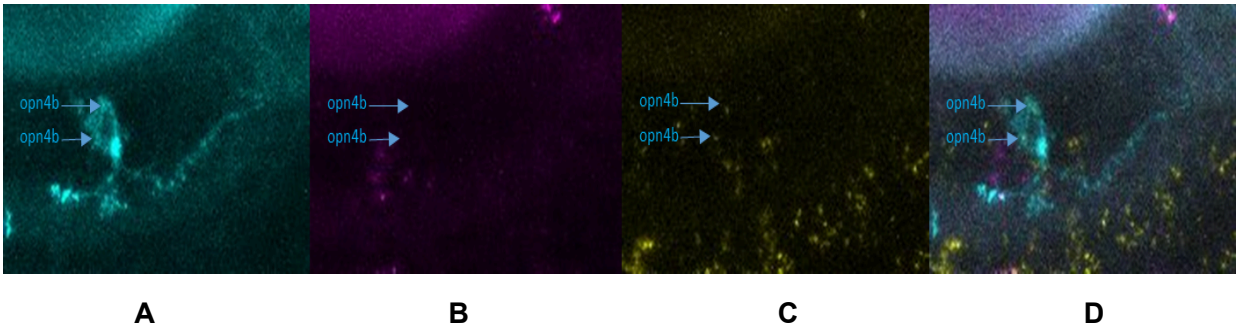

Fig.24: (D) Monostratified *eomesa*+ RGC labelled with GFP (A, cyan) expressing *opn4b* (C, yellow depicting the 647 nm HCR hairpin specific for *opn4b*) but not *opn4xa* (B, magenta depicting the 546 nm HCR hairpin specific for *opn4xa*)..

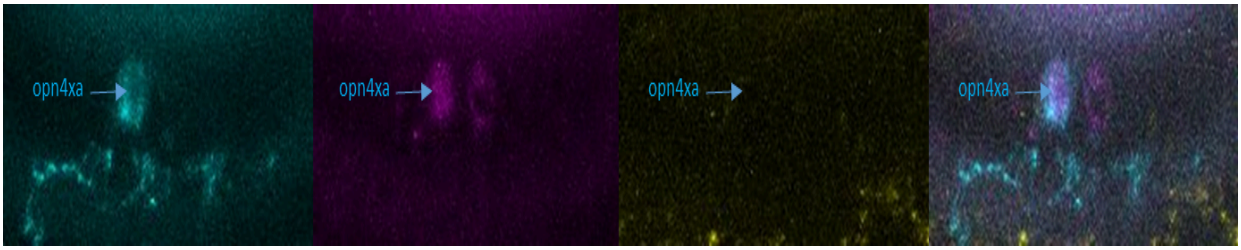

A **B** **C** **D**

Fig.25: (D) Monostratified *eomesa*+ RGC labelled with GFP (A, cyan) expressing *opn4xa* (B, magenta depicting the 546 nm HCR hairpin specific for *opn4xa*) but not *opn4b* (C, yellow depicting the 647 nm HCR hairpin specific for *opn4b*).

Three types of monostratified *eomesa*+ RGCs were observed based on gene expression patterns. There were monostratified RGCs that expressed both the opsins, *opn4xa* and *opn4b* and those that expressed either of the opsins exclusively: *opn4xa* or *opn4b*. This suggests that monostratified *eomesa*+ RGCs express opsins of both (Fig.23) or either type (Fig.24 and 25), and potentially are ipRGCs.

3.2.2. HCRs for *onecut1* on *eomesa*+ RGCs reveal monostratified dendritic stratification

To understand the morphology of *eomesa*+ *onecut1*+ RGCs, *in-situ* HCR for *onecut1* was performed on sparsely labelled *eomesa*+ RGCs. Out of the 14 Mono3 monostratified *eomesa*+ RGCs identified, 10 of them expressed *onecut1* (Fig. 26) while four of them did not.

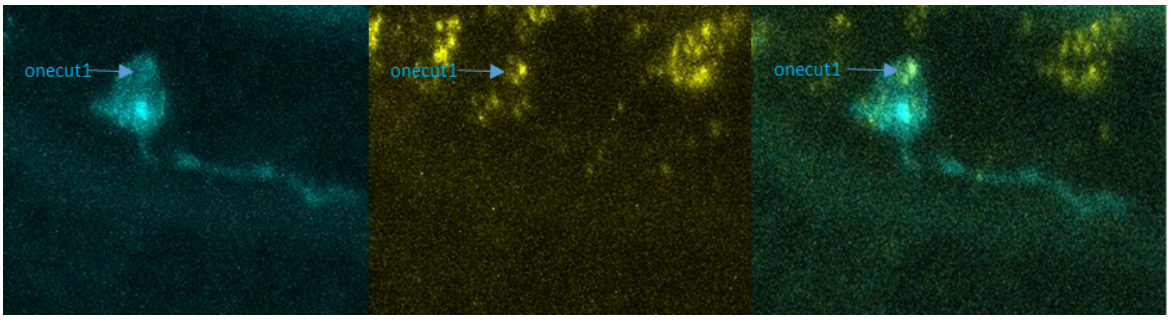

A **B** **C**

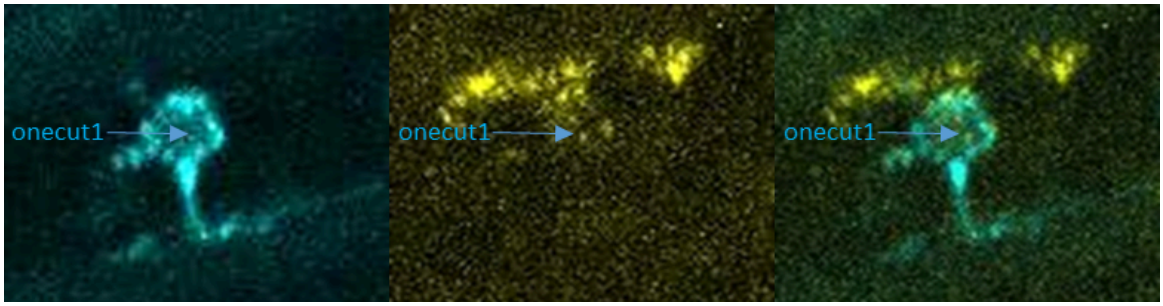

Fig. 26: (C and F) Single *eomesa*+ Mono3 monostratified RGCs labelled with GFP (A and D, cyan) expressing *onecut1* (B and E, yellow depicting the 647 nm HCR hairpin specific for onecut1).

Apart from validating the presence of *onecut1*+ *eomesa*+ Mono3 monostratified RGCs, this also suggests that *eomesa*+ RGCs that do not express *onecut1* can still belong to the Mono3 monostratified RGC population.

3.2.3. HCRs for *onecut1* and *eomesa* on *tbx20*+ RGCs reveal that all *tbx20*+ RGCs are monostratified, but not all express both *eomesa* and *onecut1*

The transcriptomic data from Kölsch et al (2021)[1] suggest that RGCs of LC4 express *tbx20, eomesa* and *onecut1* as well as *opn4xa* and *opn4b*. Further, *tbx20* neurons were shown to be a uniform group with dendrites monostratified on the ON layer of the IPL and with axonal projections arborizing in AF4 and AF9. We were interested in investigating if all *tbx20* RGCs express *onecut1* and *eomesa*, making LC4 a homogenous cell cluster with tbx20 as a common marker. To analyze this, *in situ* HCR for *eomesa* and *onecut1* was performed on labelled *tbx20*+ RGCs using *tbx20:Gal4 UAS:Dendra* transgenic line.

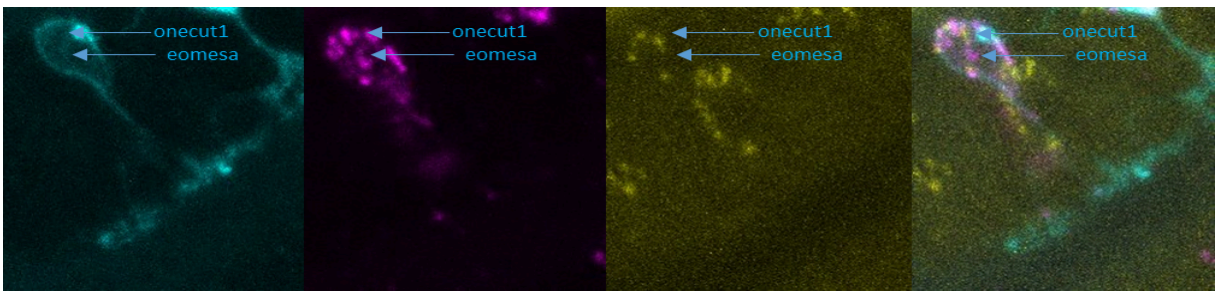

Fig. 27: (D) Monostratified *tbx20*+ RGCs labelled with GFP (A, cyan) expressing both *eomesa* (magenta depicting the 564 nm HCR hairpin specific for *eomesa*) and *onecut1* (yellow depicting the 647 nm HCR hairpin specific for *onecut1*).

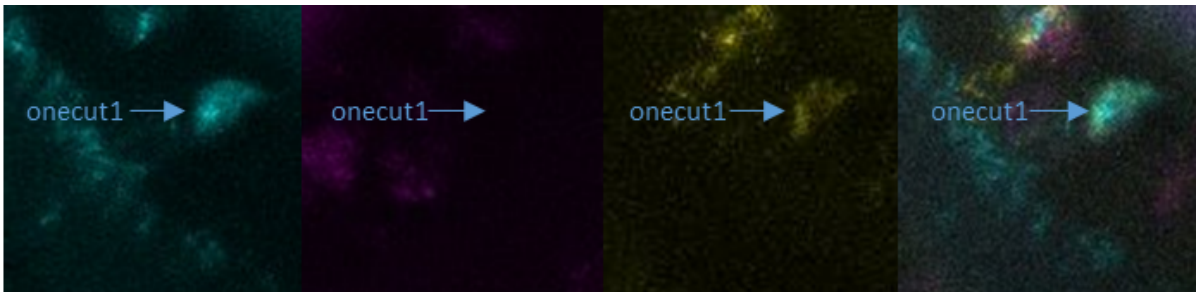

Fig. 28: (D) Monostratified *tbx20+* RGCs labelled with GFP (A, cyan) expressing *onecut1* (yellow depicting the 647 nm HCR hairpin specific for *onecut1*) but not *eomesa* (magenta depicting the 564 nm HCR hairpin specific for *eomesa*).

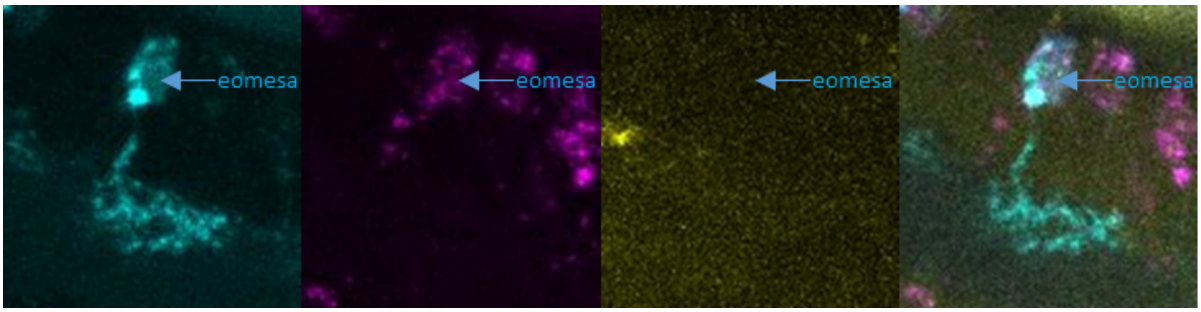

Fig. 29: (D) Monostratified *tbx20+* RGCs labelled with GFP (A, cyan) expressing *eomesa* (magenta depicting the 564 nm HCR hairpin specific for *eomesa*) but not *onecut1* (yellow depicting the 647 nm HCR hairpin specific for *onecut1*).

On the analysis of 57 *tbx20+* RGCs, it was found that 70% of the cells expressed both *eomesa* and *onecut1* (Fig.27). About 12% of the cells expressed only *eomesa* (Fig.29) while a small fraction of about 5% expressed only *onecut1* (Fig.28). About 12% of *tbx20+* cells expressed neither *eomesa* nor *onecut1* suggesting that the expression of *eomesa* and *onecut1* was very low in some of these RGCs. All the cells were monostratified depicting Mono3 and Mono4 dendritic stratification as expected.

The HCR staining also revealed many cells showing an overlap of *eomesa* and *onecut1* expression but not *tbx20*. This could either indicate that the *tbx20:Gal4 UAS:Dendra* does not label all the *tbx20* RGCs or that there is a significant proportion of *eomesa+ onecut1+* RGCs that do not express *tbx20*. Combining these results leads us to the inference that the larval cluster, LC4, contains a more heterogeneous population of RGCs than expected.

3.2.4. The different eomesa+ RGC morphotypes could be correlated to their transcriptomic types based on the *in situ* HCR results

Inferences from the *in situ* HCR results can be used to preliminarily map the *eomesa*+ RGC morphotypes to their transcriptomic types. Results from Section 3.2.1 reveal insights on opsin-expressing *eomesa*+ RGCs. The bistratified *eomesa*+ *opn4xa*- *opn4b*- RGCs presumably belong to the LC13 related RGCs that do not express opsins: LC19 (*eomesa*+ *onecut1*+ RGCs) or LC25 (*eomesa*+ RGCs) or both. LC25 contains *eomesa*+ *opn4xa*- *opn4b*- RGCs and lacks an adult counterpart[1]. Our morphological catalogue of *eomesa*+ RGCs in 21 dpf old juveniles reveal the absence of Bi3 bistratified RGCs as opposed to six dpf old larvae (Section 3.1.5). Combining all the above observations, it is likely that LC25 contains Bi3 bistratified RGCs. However, more RGCs from 21 dpf old juveniles are needed to come to a statistically significant conclusion.

There were also Mono3/Mono4 monostratified *eomesa*+ RGCs which expressed both the opsins, *opn4xa* and *opn4b*. These RGCs could belong to the opsin containing *eomesa*+ RGC larval clusters, LC18 or LC4 or both. This inference is concurrent with the fact that LC4 is known to contain Mono3 and Mono4 monostratified dendritic morphotypes[1]. There were also Mono3/Mono4 monostratified *eomesa*+ RGCs that expressed only either *opn4b* or *opn4xa.* This suggests that some of the LC26 RGCs that exclusively express *opn4b* apart from *eomesa* are monostratified. LC13 which predominantly expresses opn4xa apart from *eomesa* also contain Mono3/Mono4 monostratified RGCs.

In-situ HCR for *onecut1* on *eomesa*+ RGCs (Section 3.2.2) revealed the presence of Mono3/Mono4 monostratified RGCs that express *eomesa* but not *onecut1.* These RGCs could belong to *eomesa*+ *onecut1*- LCs like LC18, LC25, LC26. This is concurrent with the inference that LC18 and LC26 could contain monostratified RGCs based on the presence of opsins (Section 3.2.1). They could also belong to a subgroup of Mono3/Mono4 monostratified RGCs of LC4 that express *eomesa* but not *onecut1* (Section 3.3.3).

Larval cluster	Gene expression	Matching Dendritic stratification (based on HCR)
LC13	*eomesa, onecut1, tbx20, opn4xa*	Monostratified: Mono3, Mono4
LC4	*eomesa, onecut1, tbx20, opn4xa, opn4b*	Monostratified: Mono3, Mono4
LC18	*eomesa, opn4xa, opn4b*	Monostratified: Mono3, Mono4
LC19	*eomesa, onecut1*	Bistratified: Bi1, Bi3
LC25	*eomesa*	Bistratified: Bi3, Monostratified: Mono3, Mono4
LC26	*eomesa, opn4b*	Monostratified: Mono3, Mono4

Table 7: Table summarizing the preliminary conclusions on the LC13 related LCs and their morphology.

It is apparent that *eomesa*+ RGCs are predominantly Mono3/Mono4 monostratified showing five different kinds of axonal projection patterns (Section 3.1.3). In addition to this, conclusions from the *in situ* HCRs also suggest that *eomesa*+ RGCs with Mono3/Mono4 monostratified dendritic morphology also show about five different gene expression patterns (Table 7). To identify if each axonal projection pattern of Mono3/Mono4 *eomesa*+ RGCs correspond to specific transcriptomic types, Cre transgenic lines, enabling the intersectional labelling of different LC13 related clusters, need to be generated to catalogue their morphology. For example, to target LC26 which exclusively express *opn4b* apart from *eomesa*, *opn4b-Cre* construct is to be injected into fish of genotype *eomesa:QF2 QUAS:switch-epNTR-tagRFP* so that the *eomesa+*

opn4b+ RGCs are labelled with RFP. This will hopefully enable morphological studies on the different transcriptomic subypes of *eomesa*+ RGCs.

3.3. Relevance of *eomesa*+ and *onecut1*+ RGCs in phototaxis

3.3.1. Chemogenetic ablation of *eomesa*+ RGCs lead to phototactic defect in 7 dpf old zebrafish larvae

The transcriptomic data in Kölsch et al (2021)[1] revealed that some *eomesa*+ RGCs express opsins similar to ipRGCs. This could suggest that like ipRGCs, *eomesa*+ RGCs could be involved in non-image forming functions like phototaxis, circadian rhythm regulation and pigmentation.[1][40] To more closely understand the involvement of the different transcriptomic types of *eomesa*+ RGCs in phototaxis, chemogenetic ablation of these RGCs was performed with 2 mM Ronidazole before subjecting these fish to a closed-loop phototaxis assay. In Kölsch et al. (2021)[1], the phototaxis assay was done with an open-loop setup. This includes a light-dark arena with light illuminated in a fixed half of the petri dish. The trajectory of the fish in this arena was thereafter analyzed for conclusions. Using such conditions, it was shown that the *eomesa*+ RGCs are important for the positive phototaxis seen in zebrafish larvae. In this project, a closed-loop setup is used in which the projection of light is adjusted as the fish moves such that only one half of the fish is illuminated at all points of time. The polarity, i.e, left vs right, of this illumination is changed after 300 seconds. This is a more robust approach as the fish is subjected to the decision making towards light at every point in time. To validate the closed-loop setup, the phototactic defect of seven dpf larvae with *eomesa*+ RGCs ablated was tested as positive control.

The fish were subjected to bright conditions in the arena for acclimatization for 300 seconds. The light stimuli was shone on the right half of the fish for the next 300 seconds and to the left half of the fish for the following 300 seconds. The angle of the fish wasderived from the tracked coordinates of the fish at every time frame. The cumulative angle was plotted against time for analysis. Negative values of cumulative angle represent the fish moving towards right while positive values represent movement of the fish towards left.

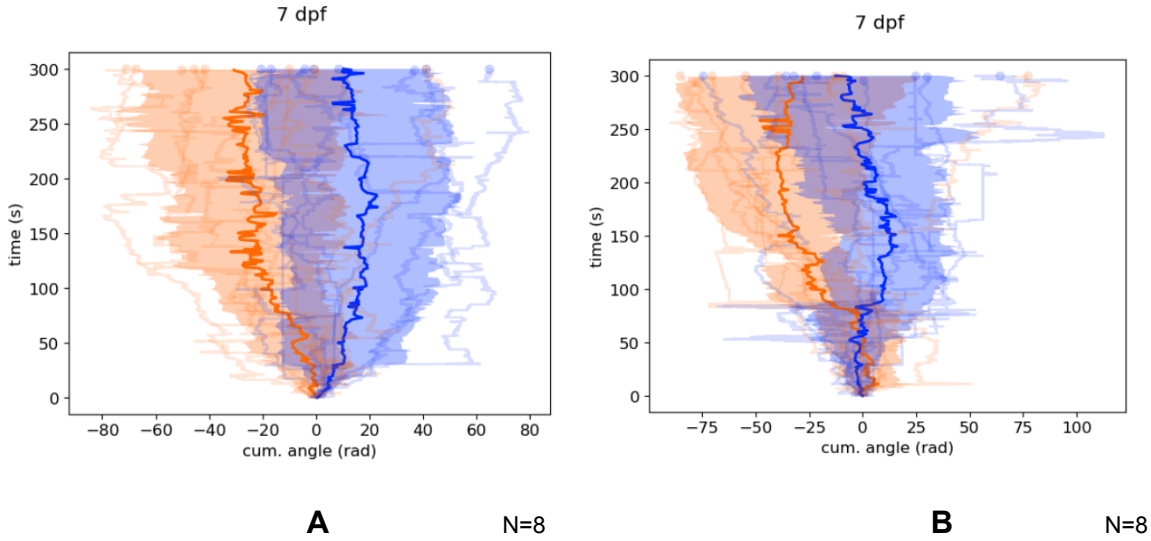

Fig. 30: (A) Cumulative angle (radians) vs time plot (seconds) for *ath5:Cre eomesa:QF2 QUAS:switchNTR* fish subjected to 0.1% DMSO (controls). N=8. (B) Cumulative angle vs time plot for the *ath5:Cre eomesa:QF2 QUAS:switchNTR* fish subjected to 2 mM Ronidazole in 0.1% DMSO (experiment). N=8. Thicker lines represent the average of the thinner lines which represent individual fish.

In Fig.30, the orange lines were plotted for the first 300 seconds when the light stimulus was on the right and the blue lines represent the latter 300 seconds when the light stimulus was on the left. The fish administered to only 0.1% DMSO show already from the start a clear separation between the average orange and blue lines suggesting that they prefer turning towards the right side when the light was on the right and left turns when the light was on the left, showing clear phototactic abilities. However, in fish subjected to 2 mM ronidazole in 0.1% DMSO, several blue lines have a negative slope indicating that some of the fish turned right when the light was on their right half. Hence, a defect in phototactic abilities was observed after ablation of *eomesa*+ RGCs.

3.3.2. Chemogenetic ablation of *onecut1*+ RGCs lead to phototactic defect in 7 dpf old zebrafish larvae

Since it has been established that *eomesa*+ RGCs play a role in phototaxis by section 3.3.1 and in Kölsch et al. (2021), we were interested in narrowing down on which transcriptomic subtypes of the *eomesa*+ RGCs contribute to this behavior. Subclusters of *eomesa*+ RGCs like those belonging to LC4 also express *onecut1.* To investigate if

onecut1 ablation also affects phototaxis, the chemogenetic ablation with 2 mM Ronidazole and the phototaxis assay was replicated on *ath5:Cre onecut1:QF2 QUAS:switchNTR*.

Interestingly, ablation of *onecut1*+ RGCs also confer a clear decrease in the ability to perform phototaxis. The experiment was repeated five times with eight to ten fish each (Fig. 31). The results were reproducible with inverted polarity with light administration on the left for the first 300 seconds and on the right for the latter 300 seconds (Fig.32). Fig. 33 contains the cumulative angle (radians) vs time (seconds) graphs for individual fish as opposed to the summary graphs shown in Fig. 31 and Fig.32. Fig.33A, 33B and 33C depict individual *ath5:Cre onecut1:QF2 QUAS:switchNTR* fish subjected to 0.1% DMSO (control). The fish are kept in brightly lit conditions for the first 300 seconds for acclimatization purposes. Followed by this, light was administered only to the right half of the fish from 300 to 600 seconds where the graph has a negative slope meaning the fish turned right. In the time interval of 600 to 900 seconds when light was administered to the left of the fish, the graph has a positive slope meaning the fish were turning to the left. Therefore, the controls clearly show phototaxis with an apparent switch at the 600th second with the switch in light polarity. In Fig. 33D, 33E and 33F, the graphs depict individual *ath5:Cre onecut1:QF2 QUAS:switchNTR* fish subjected to 2mM Ronidazole in 0.1% DMSO (chemogenetic ablation). It is apparent that the slopes of the graphs are either positive or negative through the entire time period suggesting that the fish kept turning to the left or to the right regardless of where light is administered.

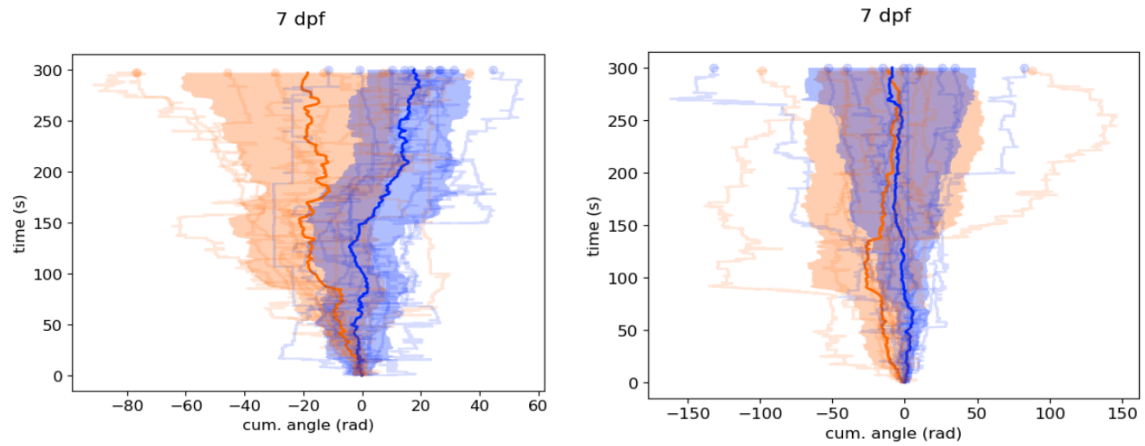

A N=10 **B** N=10

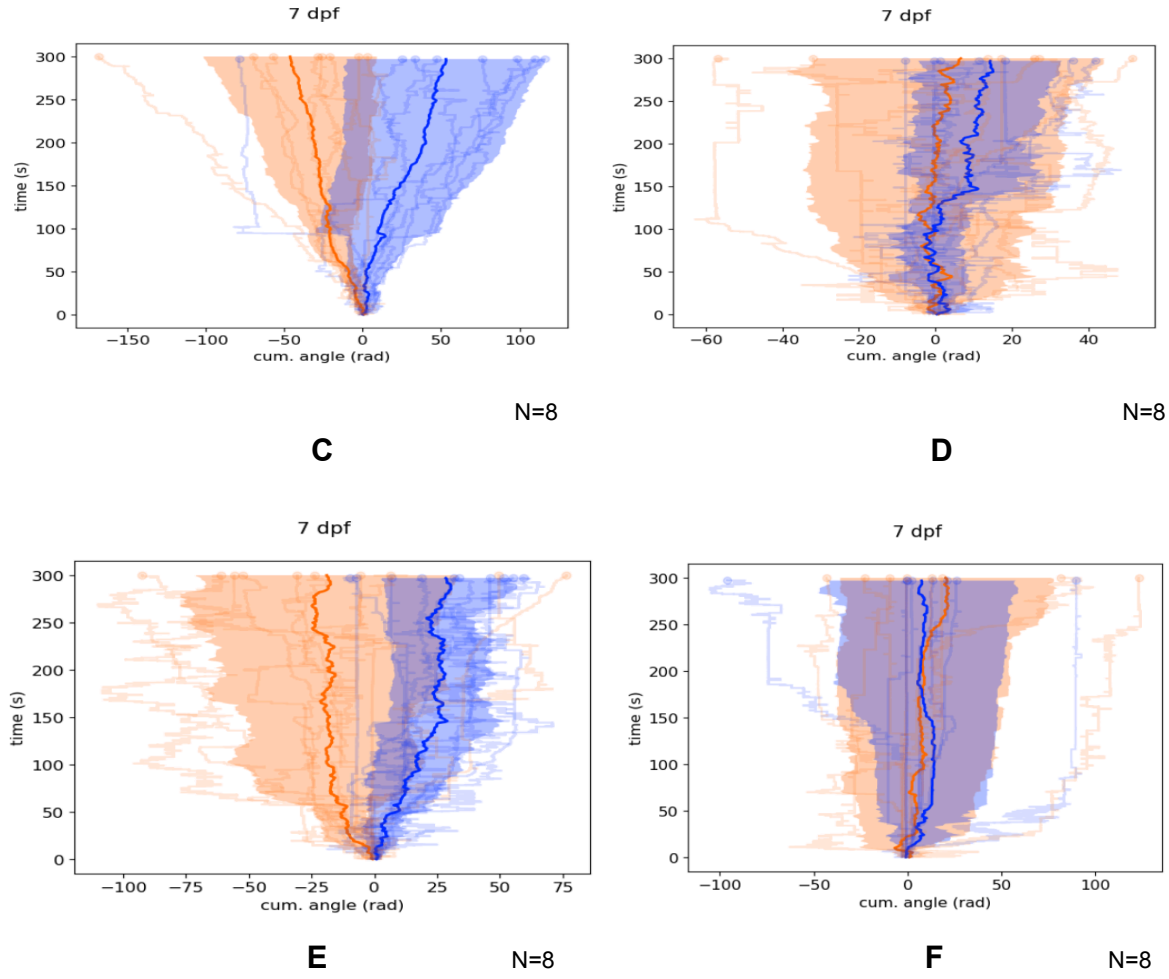

Fig.31: (A, C, E) Cumulative angle (radians) vs time plot (seconds) for *ath5:Cre onecut1:QF2 QUAS:switchNTR* fish subjected to 0.1% DMSO (controls). (B, D, F) Cumulative angle vs time plot for the *ath5:Cre onecut1:QF2 QUAS:switchNTR* fish subjected to 2 mM Ronidazole in 0.1% DMSO (experiment).

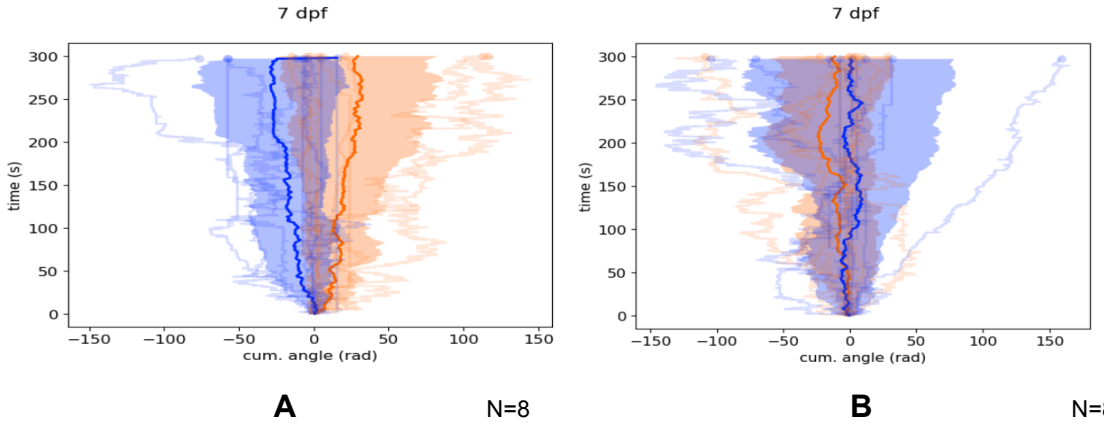

Fig.32: (A) Cumulative angle (radians) vs time plot (seconds) for *ath5:Cre onecut1:QF2 QUAS:switchNTR* fish subjected to 0.1% DMSO (controls). (B) Cumulative angle vs time plot for the *ath5:Cre onecut1:QF2 QUAS:switchNTR* fish subjected to 2 mM Ronidazole in 0.1% DMSO (experiment). The polarity in this experiment is inverted with light stimuli on the left of the fish for the first 300 sec and to the right of the fish for the next 300 sec.

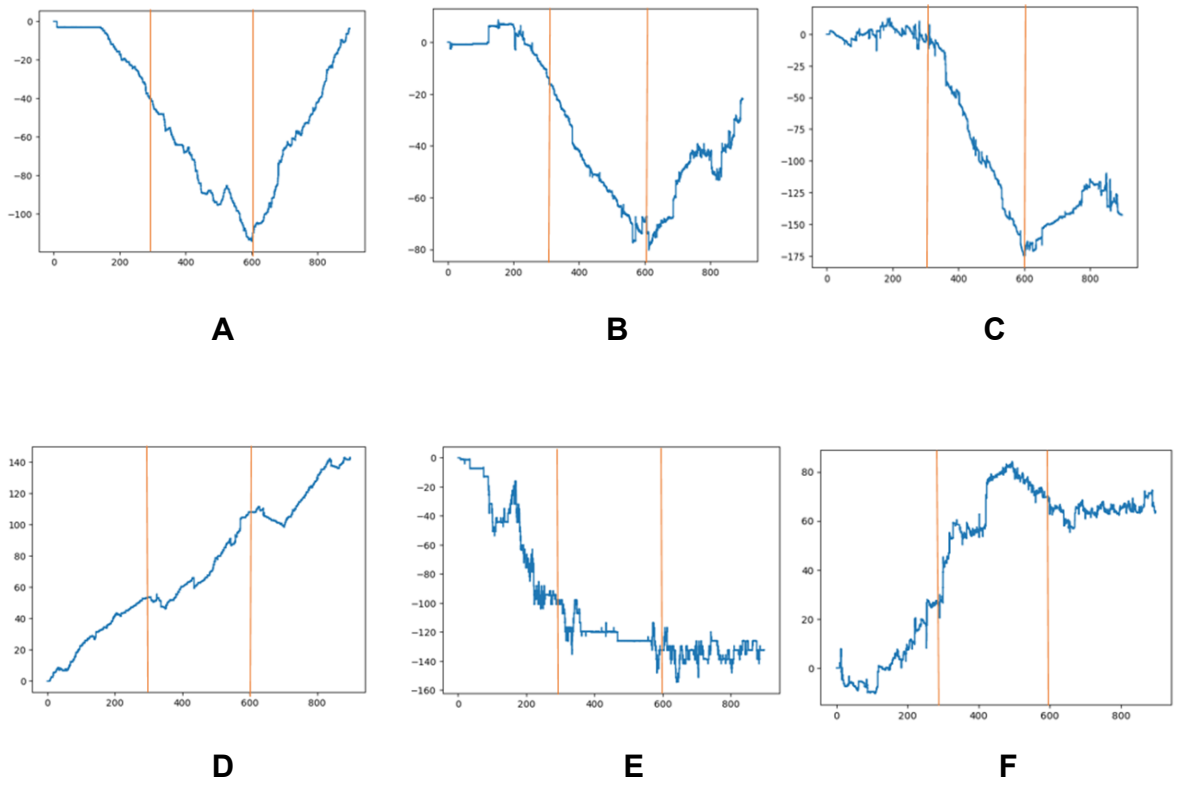

Fig.33: Cumulative angle in radians (y-axis) and time in seconds (x-axis) for individual *ath5:Cre onecut1:QF2 QUAS:switchNTR* fish subjected to (A,B,C) 0.1% DMSO and (D,E,F) 2mM Ronidazole in 0.1% DMSO.

As opposed to the ablation of the *eomesa*+ RGCs, the phototactic defect in the case of *onecut1*+ ablation is rather dramatic. Combining the two results, a conclusion would be that the cluster that expresses both *eomesa* and *onecut1,* LC4 might be involved in phototaxis. LC4 is the larval cluster mainly containing the *eomesa*+ *onecut1*+ *tbx20*+ RGCs. To validate the hypothesis that *eomesa*+ *onecut1*+ *tbx20*+ RGCs are involved in phototaxis, this assay has to be repeated on the ablation of *tbx20*+ RGCs. The transgenic line, *tbx20: Gal4 UAS: NTR* can be used for this purpose. To specifically target these *onecut1*+ *eomesa*+ RGCs, the Cre line, *onecut1:Cre eomesa:QF2 QUAS:switchNTR*, is also being generated using the CRISPR knockin method.

If the ablation of *tbx20*+ RGCs show a dramatic decrease in phototactic abilities, this would suggest that it is the *eomesa*+ *onecut1*+ *tbx20*+ RGC subpopulation that contribute mainly to phototaxis. However, there is a possibility that *tbx20*+ RGCs do not show significant phototactic defects. Since *tbx20*+ RGCs do not project to regions like

AF1 and AF2 which could be involved in phototaxis, it is likely that *tbx20*+ RGCs do not contribute to phototaxis at all. This would suggest two possibilities. Since LC4 is a more heterogeneous population than expected, opsin containing *eomesa*+ *onecut*+ RGCs that do not express *tbx20* might be involved in phototaxis. It might also be the case that *eomesa*+ RGCs and *onecut1*+ RGCs play independent but complementary roles in this navigational behavior towards light.

3.4. Conclusion and Future Outlook

In summary, since it is known that the larval and adult transcriptomic RGC types in zebrafish are greatly different[1], the broad objective of this project was to understand whether the developmental processes in RGCs follow the remodeling or replacement model. Following morphological changes of RGCs over time is one way of obtaining significant insights on their development. To achieve this, this project attempted at mapping different *eomesa*+ RGC transcriptomic types to their corresponding morphotypes.

Morphological characterization of *eomesa*+ RGCs in six dpf larvae revealed six different morphotypes based on dendritic morphology and seven different morphotypes based on axonal projection patterns. In comparison, only five different dendritic morphotypes were identified in the case of 21 dpf old juveniles. It has also been shown that the abundance of *eomesa*+ RGCs decreases over the course of development. This established that the number and morphological subtypes of RGCs change with time in accordance with transcriptomic changes. Following this, *in-situ* HCRs are performed on *eomesa*+ RGCs to integrate insights on gene expression patterns exhibited by various morphotypes. This offered preliminary matching of the transcriptomic RGC types to their morphology. In addition to this extensive analysis on morphological development, to understand the functional relevance of *eomesa*+ transcriptomic subtypes, a phototaxis assay was performed post ablation of *eomesa*+ and *onecut1*+ RGCs. It showed that both of these RGCs contribute to the phototactic abilities seen in seven dpf old larvae.

This project will be further developed by targeting individual larval subclusters of *eomesa*+ RGCs using an intersectional approach with interesting Cre recombinase expressing lines currently being made. This will aid in in-depth analysis of the

subclusters' morphology and functional relevance. Apart from the analysis of morphological aspects of these RGCs over different developmental stages in fixed fish, morphology of a singly labelled RGC in a live fish will be tracked over time. This will give us a more accurate understanding of RGC morphotype development. The phototaxis assay can be performed post chemogenetic ablation on fish expressing NTR in specific LC13 related RGCs to narrow down on the clusters contributing to this behavior. This will enable us to develop a more comprehensive understanding of RGC type development and their functional consequences.

Supplementary

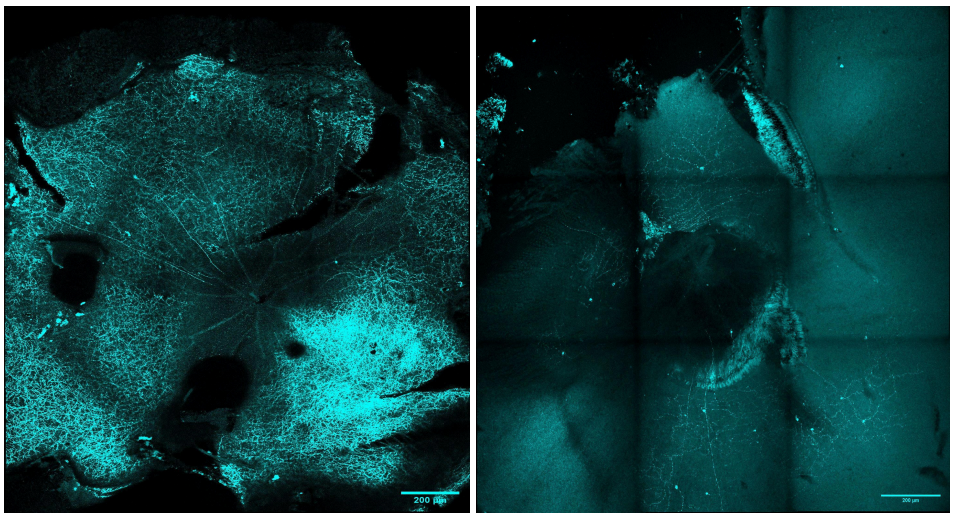

A **B**

Fig. S1: Confocal images of retinal flatmounts of (A) *eomesa:QF2 QUAS:tagRFP* and (B) *tbx20:Gal4 UAS:Dendra* adults showing the axons of RGCs converging in the optic nerve in the center. Three significant bundles of axons are visible in (A) and (B) suggesting comparable abundance.

References

1. Kölsch Y, Hahn J, Sappington A, Stemmer M, Fernandes AM, Helmbrecht TO, Lele S, Butrus S, Laurell E, Arnold-Ammer I, Shekhar K, Sanes JR, Baier H. Molecular classification of zebrafish retinal ganglion cells links genes to cell types to behavior. Neuron (2021) and Molecular Dissection of the Retinal Projectome submitted by Yvonne Kölsch (2019).
2. Robles E, Laurell E, Baier H. The retinal projectome reveals brain-area-specific visual representations generated by ganglion cell diversity. Curr Biol (2014).
3. Masland, R. H. Neuronal cell types. Curr. Biol. 14, R497–R500 (2004)
4. Dowling, J. The Retina - an approachable part of the brain (1987).
5. Kolb, H. How the retina works. Am. Sci. 91, 28–35 (2003).
6. Portugues, R. & Engert, F. The neural basis of visual behaviors in the larval zebrafish. Curr. Opin. Neurobiol. 19, 644–647 (2009).
7. Sanes, J. R. & Zipursky, S. L. Design Principles of Insect and Vertebrate Visual Systems. Neuron 66, 15–36 (2010).
8. Fleisch VC, and Neuhauss SCF. Visual Behavior in Zebrafish. Zebrafish 3, 191–201. (2006)
9. Veldman, M., Lin, S. Zebrafish as a Developmental Model Organism for Pediatric Research. *Pediatr Res* 64, 470–476 (2008).
10. Masland, R. H. The fundamental plan of the retina. Nat. Neurosci. 4, 877–886 (2001).
11. Masland, R. H. The Neuronal Organization of the Retina. Neuron 76, 266–280 (2012).
12. Fish Physiology 29, Academic Press (2010)
13. Amini R, Rocha-Martins M, Norden C. Neuronal Migration and Lamination in the Vertebrate Retina. Front Neurosci. 2018
14. Nawrocki, L., BreMiller, R., Streisinger, G. & Kaplan, M. Larval and adult visual pigments of the zebrafish, Brachydanio rerio. Vision Res. 25, 1569–76 (1985).
15. Marc, R. & Cameron, D. A molecular phenotype atlas of the zebrafish retina. J. Neurocytol. 30, 593–654 (2002).
16. Li, Y. N., Tsujimura, T., Kawamura, S. & Dowling, J. E. Bipolar cell-photoreceptor connectivity in the zebrafish (Danio rerio) retina. J. Comp. Neurol. 520, 3786–3802 (2012).
17. Euler, T., Haverkamp, S., Schubert, T. & Baden, T. Retinal bipolar cells: elementary building blocks of vision. Nat. Rev. Neurosci. 15, 507–19 (2014).
18. Connaughton, V. P., Graham, D. & Nelson, R. Identification and morphological classification of horizontal, bipolar, and amacrine cells within the zebrafish retina. J. Comp. Neurol. 477, 371–385 (2004).
19. Vitorino, M. et al. Vsx2 in the zebrafish retina: Restricted lineages through derepression. Neural Dev. 4, (2009).
20. Song, P., Matsui, J. & Dowling, J. E. Morphological types and connectivity of horizontal cells found in the adult zebrafish retina. J. Comp. Neurol. 506, 287–297 (2008).

21. Twig, G., Levy, H. & Perlman, I. Color opponency in horizontal cells of the vertebrate retina. Prog. Retin. Eye Res. 22, 31–68 (2003).
22. Connaughton, V. P. & Nelson, R. Spectral Responses in Zebrafish Horizontal Cells Include a Tetraphasic Response and a Novel UV-Dominated Triphasic Response. J. Neurophysiol. 104, 2407–2422 (2010).
23. Macneil, M. A. & Masland, R. H. Extreme Diversity among Amacrine Cells: Implications for Function. Cell 20, 971–982 (1998).
24. Jusuf, P. R. & Harris, W. a. Ptf1a is expressed transiently in all types of amacrine cells in the embryonic zebrafish retina. Neural Dev. 4, 34 (2009).
25. Gollisch, T. & Meister, M. Eye Smarter than Scientists Believed: Neural Computations in Circuits of the Retina. Neuron 65, 150–164 (2010).
26. Olveczky BP, Baccus SA, Meister M. Retinal adaptation to object motion. Neuron. 2007
27. Zhao, X., Chen, H., Liu, X. & Cang, J. Orientation-selective Responses in the Mouse Lateral Geniculate Nucleus. J. Neurosci. 33, 12751–12763 (2013).
28. Burrill JD, Easter SS Jr. Development of the retinofugal projections in the embryonic and larval zebrafish (Brachydanio rerio). J Comp Neurol (1994).
29. Xiao, T., Roeser, T., Staub, W. & Baier, H. A GFP-based genetic screen reveals mutations that disrupt the architecture of the zebrafish retinotectal projection. *Development* 132, 2955–2967 (2005).
30. Baier H, Wullimann MF. Anatomy and function of retinorecipient arborization fields in zebrafish. J Comp Neurol. (2021).
31. Karlstrom, R. O., Trowe, T. & Bonhoeffer, F. Genetic analysis of axon guidance and mapping in the zebrafish. Trends Neurosci. 20, 3–8 (1997).
32. Semmelhack, J. L. et al. A dedicated visual pathway for prey detection in larval zebrafish. Elife 3, (2014).
33. Guler et al 2007
34. Panda S, Provencio I, Tu DC, Pires SS, Rollag MD, Castrucci AM, Pletcher MT, Sato TK, Wiltshire T, Andahazy M, Kay SA, Van Gelder RN, Hogenesch JB. Melanopsin is required for non-image-forming photic responses in blind mice. Science (2003).
35. ZFIN: Eomesa gene: https://zfin.org/ZDB-GENE-001228-1#
36. Chen CK, Kiyama T, Weber N, Whitaker CM, Pan P, Badea TC, Massey SC, Mao CA. Characterization of Tbr2-expressing retinal ganglion cells. J Comp Neurol. (2021).
37. Peng, Y.-R. et al. Molecular Classification and Comparative Taxonomics of Foveal and Peripheral Cells in Primate Retina. Cell 176, 1–16 (2019).
38. Do, M. T. H. & Yau, K.-W. Intrinsically photosensitive retinal ganglion cells. Physiol. Rev. 90, 1547–1581 (2010).
39. Fiske, S. et al. Circadian photoreception in the retinally degenerate mouse (rd/rd). J. Comp. Physiol. A 169, 39–50 (2004).
40. Freedman, M. S. et al. Circadian behavior by non-rod, non-cone, ocular photoreceptors. Science (80-.). 284, 502–504 (1999).
41. Hattar, S. et al. Melanopsin-Containing Retinal Ganglion Cells: Architecture, Projections, and Intrinsic Photosensitivity. Science (80-.). 295, 1065–1070 (2002).
42. Schmidt TM, Chen SK, & Hattar S (2011). Intrinsically photosensitive retinal ganglion cells: many subtypes, diverse functions. Trends Neurosci, (2011).

43. Do, M. T. H. Melanopsin and the intrinsically photosensitive retinal ganglion cells: Biophysics to behavior. *Neuron* 104, 205–226 (2019).
44. Wong KY. A retinal ganglion cell that can signal irradiance continuously for 10 hours. J Neurosci. (2012)
45. Davies, W. I. et al. Functional diversity of melanopsins and their global expression in the teleost retina. *Cell. Mol. Life Sci.* 68, 4115–4132 (2011).
46. Mao, C.-A. et al. T-box Transcription Regulator Tbr2 Is Essential for the Formation and Maintenance of Opn4/Melanopsin-Expressing Intrinsically Photosensitive Retinal Ganglion Cells. J. Neurosci. 34, 13083–13095 (2014).
47. N. T., Tierney, H. & Feldheim, D. A. Tbr2 Is Required to Generate a Neural Circuit Mediating the Pupillary Light Reflex. J. Neurosci. 34, 5447–5453 (2014).
48. Hatter, S. et al. Central Projections of Melanopsin- Expressing Retinal Ganglion Cells in the Mouse. J. Comp. Neurol. 497, 326–349 (2006).
49. Matos-Cruz, V. et al. Unexpected Diversity and Photoperiod Dependence of the Zebrafish Melanopsin System. PLoS One 6, e25111 (2011).
50. Thisse, C. & Thisse, B. High Throughput Expression Analysis of ZF-Models Consortium Clones (2005).
51. Lin, B., Wang, S. W. & Masland, R. H. Retinal Ganglion Cell Type , Size , Report and Spacing Can Be Specified Independent of Homotypic Dendritic Contacts. 43, 475–485 (2004).
52. Orger MB, Baier H. Channeling of red and green cone inputs to the zebrafish optomotor response. *Visual Neuroscience* (2005).
53. Serra, E. L., C. C. Medalha, and R. Mattioli. "Natural preference of zebrafish (Danio rerio) for a dark environment." *Brazilian journal of medical and biological research* 32 (1999).
54. Maximino, Caio, et al. "A comparative analysis of the preference for dark environments in five teleosts." *International Journal of Comparative Psychology* 20.4 (2007).
55. Lai S, Kumari A, Liu J, Zhang Y, Zhang W, Yen K, Xu J. Chemical screening reveals Ronidazole is a superior prodrug to Metronidazole for nitroreductase-induced cell ablation system in zebrafish larvae. J Genet Genomics (2021).
56. Riabinina O, Potter CJ. The Q-System: A Versatile Expression System for Drosophila. Methods Mol Biol (2016).
57. McLellan MA, Rosenthal NA, Pinto AR. Cre-loxP-Mediated Recombination: General Principles and Experimental Considerations. Curr Protoc Mouse Biol. (2017).
58. Tol2 mediated transgenesis: K. Kawakami, K. Asakawa, A. Muto, H. Wada, Chapter 2 - Tol2-mediated transgenesis, gene trapping, enhancer trapping, and Gal4-UAS system, Methods in Cell Biology, Academic Press,Volume 135, (2016).
59. CRISPR: Ma Y, Zhang L, Huang X. Genome modification by CRISPR/Cas9. FEBS J. (2014).
60. Choi HMT, Schwarzkopf M, Fornace ME, Acharya A, Artavanis G, Stegmaier J, Cunha A, Pierce NA. Third-generation *in situ* hybridization chain reaction: multiplexed, quantitative, sensitive, versatile, robust. Development (2018).
61. Semmelhack JL, Donovan JC, Thiele TR, Kuehn E, Laurell E, Baier H. A dedicated visual pathway for prey detection in larval zebrafish. Elife. (2014).

62. Kubo F, Hablitzel B, Dal Maschio M, Driever W, Baier H, Arrenberg AB. Functional architecture of an optic flow-responsive area that drives horizontal eye movements in zebrafish. Neuron. (2014).
63. Kramer, A., Wu, Y., Baier, H., Kubo, F. (2019) Neuronal Architecture of a Visual Center that Processes Optic Flow. Neuron. 103(1):118-132.e7.(2019).
64. MapZebrain Atlas: https://mapzebrain.org/home
65. Baver SB, Pickard GE, Sollars PJ, Pickard GE. Two types of melanopsin retinal ganglion cell differentially innervate the hypothalamic suprachiasmatic nucleus and the olivary pretectal nucleus. Eur J Neurosci. (2008).
66. D.C. Fernandez, Y.T. Chang, S. Hattar, S.K. Chen. Architecture of retinal projections to the central circadian pacemaker. Proc. Natl. Acad. Sci. USA, 113 (2016).